An International Journal of Optimization and Control: Theories & Applications
ISSN: 2146-0957 eISSN: 2146-5703
Vol.16, No.1, pp.205-231 (2026)
https://doi.org/10.36922/IJOCTA025390160

RESEARCH ARTICLE

Fractional dynamics and cost-effective control strategies for measles transmission

Asiyeh Ebrahimzadeh[1] and Amin Jajarmi[2,3*]

[1]Department of Mathematics, Faculty of Education and Graduate Studies, Farhangian University, Tehran, Iran
[2]Department of Electrical Engineering, University of Bojnord, P.O. Box, 94531-1339, Bojnord, Iran
[3]Department of Mathematics, Saveetha School of Engineering, SIMATS, Saveetha University, Chennai 602105, Tamil Nadu, India
a.ebrahimzadeh@cfu.ac.ir, a.jajarmi@ub.ac.ir

ARTICLE INFO

Article History:
Received: September 23, 2025
Revised: November 3, 2025
Accepted: November 10, 2025
Published Online: December 16, 2025

Keywords:
Fractional epidemic model
Measles transmission
Vaccination behavior
Optimal control
Memory effects
Cost-effectiveness analysis

ABSTRACT

Despite the proven effectiveness of measles vaccines, suboptimal coverage and changing public behavior continue to pose challenges for eradication efforts worldwide. This study develops a fractional-order compartmental model to capture measles transmission dynamics while accounting for memory effects and adaptive behavioral responses to vaccination campaigns. Using Caputo fractional derivatives, the model reflects the non-local and history-dependent nature of disease spread more realistically than classical integer-order models. Four time-dependent control strategies—early newborn vaccination, adult catch-up immunization, administration of a second vaccine dose, and early treatment of exposed individuals—are incorporated and optimized through Pontryagin's Maximum Principle adapted for fractional systems. A sensitivity analysis of the basic reproduction number shows which parameters have the biggest effect on the potential for an outbreak. Numerical simulations demonstrate that fractional dynamics significantly modify infection peaks, outbreak duration, and total intervention costs compared to classical models. The results emphasize that integrating memory effects and behavioral feedback can enhance the design of vaccination programs and inform more cost-effective public health policies for measles mitigation.

1. Introduction

Measles remains among the most contagious vaccine-preventable viral diseases, and an ongoing risk to public health globally, even with the availability of safe and effective vaccines. In 2018 alone, there were over 140,000 measles-attributed deaths, primarily among children under the age of five. [1] Although massive vaccination drives have significantly reduced measles cases worldwide, occasional outbreaks still occur due to suboptimal immunization coverage rates, low health system capacity, and the increasing reality of vaccine hesitancy. [2–5] Widespread outbreaks have been reported even in regions that had already achieved elimination status, which highlights the fragility of herd immunity. [4,6]

Vaccine hesitancy, i.e., delay in the adoption or refusal of vaccination even where they are available, has emerged as a key determinant for measles eradication. [7] Misinformation, perception of low disease risk, lack of trust in health authorities, and sociocultural factors only add strength to the position and create feedback mechanisms influencing behavior around vaccination over time. [8] Thus, sophisticated modeling schemes that can capture not just the biological dynamics of measles transmission but also the adaptive behavior response of the population to vaccination policy are a pressing necessity.

*Corresponding Author

Mathematical modeling plays a central role in the investigation of disease transmission and the support of evidence-based public health interventions. Classical compartmental models formulated by integer-order differential equations have been extensively used to study measles transmission and evaluate immunization measures. [9,10] The models generally rely on the assumption that the rate of change depends solely on the current state, without accounting for memory and hereditary features that exist in biology and human behavior. To overcome this limitation, researchers have proposed fractional-order models as effective alternatives that incorporate memory features and long-range time correlations, reflecting the more realistic conditions of actual processes. [11–16]

Fractional-order differential equations—especially the Caputo type—have gained increasing interest over recent years in modeling infectious disease, for which non-locality effects and memory play an important role. [17–21] For measles and other diseases, waning immunity, variations in uptake of vaccination, and changes in behavior due to perceived risk have been outlined as the major parameters highlighting the necessity of accounting for such phenomena in predictive models. [22,23] The Atangana–Baleanu–Caputo derivative and other fractional operators have proved increased capacity for describing sub-exponential growth and multi-dimensional transmission patterns in epidemics. [23,24] Nevertheless, the majority of existing fractional-order models of measles do not consider the explicit inclusion of behavioral reactions to vaccination, despite visible evidence that behavior plays a significant role in the determination of immunization coverage. [7,8,25] Furthermore, although optimal control theory has widely been employed to construct cost-saving intervention strategies in conventional models, [26–28] its application to the context of fractional-order systems with adaptive feedback for behavior is quite understudied. [12,13,18,29]

Current studies on COVID-19, Human immunodeficiency virus, Dengue, and Monkeypox diseases have demonstrated the usefulness of combining fractional-order behavior with optimal control strategies and behavioral factors to more suitably assessing intervention effectiveness under uncertainty and resource constraints. [8,14,30–33] Such approaches enable the balance of health impacts and economic costs and facilitate decision-making for public health planning.

Inspired by gaps in existing research, this paper presents a new fractional-order model for measles transmission that includes memory effects and dynamic behavioral responses due to vaccination. The primary inquiry of this study is the impact of fractional-order dynamics and adaptive human behavior on the efficacy and cost-effectiveness of vaccination and treatment interventions in practical contexts. The model aims to help public health planners design vaccination schedules and treatment interventions that account for time delays, vaccine hesitancy, and long-term immunity. The model employs the Caputo fractional derivative of order $\alpha \in (0, 1]$ to encapsulate the hereditary characteristics of measles transmission. Four control strategies are introduced and optimized over time as follows: newborn immunization, adult catch-up vaccination, second-dose vaccination, and early treatment of exposed individuals. These strategies are optimized using a modified version of Pontryagin's Maximum Principle (PMP) for fractional systems. The basic reproduction number, $\mathcal{R}_0$, is calculated and examined using sensitivity analysis to determine the most important factors that affect the risk of an outbreak. Numerical simulations are conducted using a forward-backward sweep algorithm to compare different intervention strategies and show how fractional dynamics and behavioral feedback can significantly impact infection peaks, outbreak duration, and intervention costs. Therefore, this work connects mathematical modeling with practical policy by showing how memory effects and behavioral dynamics can be integrated into cost-effective vaccination planning. The main contributions of this work are the expansion of classical models through the use of Caputo fractional derivatives, which better capture the non-local and history-dependent nature of disease transmission, and the modeling of how individuals' behavior changes in response to vaccination policies, including vaccine hesitancy and behavior changes during outbreaks. It also uses PMP for fractional systems develop and improve the four control strategies: immunizing newborns, giving adults a second dose of the vaccine, and treating people who have been exposed to the virus early. The work also includes a comprehensive cost-effectiveness analysis that considers both the economic and health impacts of vaccination and treatment strategies, which is advantageous in public health planning. Furthermore, the study performs simulations to compare how fractional dynamics and behavioral feedback affect infection peaks, outbreak duration, and intervention costs,

showing the importance of including memory effects in epidemic models. Consequently, this work provides a framework for improving measles vaccination strategies by accounting for real-world complexities like behavioral changes and memory effects, ultimately guiding the creation of more cost-effective public health policies.

We organize the rest of this paper as follows: in Section 2, some preliminary knowledge on fractional calculus is presented, including the basic definitions and elementary properties that are required by the paper. In Section 3, the memory-based and behavioral response process is included to develop a fractional-order compartmental model for measles transmission, and the main epidemiological features, including the disease-free and endemic equilibria and the basic reproduction number, are analyzed. In Section 4, we address the optimal control problem, which includes the control system, the objective functional, and the Pontryagin necessary optimality condition formulated in the fractional sense. The numerical solutions of the fractional differential equations and corresponding simulation scenarios with comparisons are given in Section 5. Scientific interpretations of the results and policy environmental implications are discussed in Section 6, and the model outcomes are compared with equivalent classical approaches in integer orders. Finally, in Section 7, we conclude with a review and discuss possible perspectives.

2. Mathematical preliminaries

In this section, we revisit fundamental concepts and symbols related to fractional integrals and derivatives, which we utilized in this work.

Definition 1. *Let $\alpha > 0$. The left-sided Riemann–Liouville fractional integral of a function $y(t)$ is given by:* [34,35]

$$ {}^{\mathrm{R}}\mathrm{I}_t^{\alpha}\, y(t) = \frac{1}{\Gamma(\alpha)} \int_0^t (t-s)^{\alpha-1} y(s)\, ds, \quad t > 0 \tag{1} $$

where $\Gamma(\cdot)$ is the Gamma function.

Definition 2. *For $\alpha > 0$, the left-sided Riemann–Liouville fractional derivative of order α of a function $y(t)$ is defined as:* [34,35]

$$ {}^{\mathrm{R}}\mathrm{D}_t^{\alpha}\, y(t) = \frac{1}{\Gamma(n-\alpha)} \frac{d^n}{dt^n} \int_0^t (t-s)^{n-\alpha-1} y(s)\, ds \tag{2} $$

where $n = \lceil \alpha \rceil$ is the smallest integer greater than or equal to α.

Definition 3. *Let $n \in \mathbb{N}$ and $\alpha \in (n-1, n)$. The left-sided Caputo fractional derivative of order α is expressed as follows:* [34,35]

$$ {}^{\mathrm{C}}\mathrm{D}_t^{\alpha}\, y(t) = \frac{1}{\Gamma(n-\alpha)} \int_0^t (t-s)^{n-\alpha-1} y^{(n)}(s)\, ds \tag{3} $$

In particular, for $\alpha \in (0, 1)$ we obtain:

$$ {}^{\mathrm{C}}\mathrm{D}_t^{\alpha}\, y(t) = \frac{1}{\Gamma(1-\alpha)} \int_0^t (t-s)^{-\alpha} y'(s)\, ds \tag{4} $$

Definition 4. *Let $\alpha > 0$ and $0 \le t < T$. The right-sided Riemann–Liouville fractional integral is defined by:* [34,35]

$$ {}^{\mathrm{R}}\mathrm{I}_T^{\alpha}\, y(t) = \frac{1}{\Gamma(\alpha)} \int_t^T (s-t)^{\alpha-1} y(s)\, ds \tag{5} $$

Definition 5. *Let $\alpha > 0$ and $n = \lceil \alpha \rceil$. The right-sided Riemann–Liouville fractional derivative of order α is:* [34,35]

$$ {}^{\mathrm{R}}\mathrm{D}_T^{\alpha}\, y(t) = \frac{(-1)^n}{\Gamma(n-\alpha)} \frac{d^n}{dt^n} \int_t^T (s-t)^{n-\alpha-1} y(s)\, ds \tag{6} $$

Definition 6. *Let $\alpha > 0$ and $n = \lceil \alpha \rceil$. The right-sided Caputo fractional derivative is expressed as:* [34,35]

$$ {}^{\mathrm{C}}\mathrm{D}_T^{\alpha}\, y(t) = \frac{(-1)^n}{\Gamma(n-\alpha)} \int_t^T (s-t)^{n-\alpha-1} y^{(n)}(s)\, ds \tag{7} $$

Lemma 1. *Assume that the function y belongs to the space $C^n[0, T]$, where $n-1 < \alpha < n$. Then, the following identity holds:* [36,37]

$$ {}^{\mathrm{R}}\mathrm{I}_t^{\alpha}\ {}^{\mathrm{C}}\mathrm{D}_t^{\alpha}\, y(t) = y(t) - \sum_{k=0}^{n-1} \frac{y^{(k)}(0)}{k!}\, t^k \tag{8} $$

Key properties:

For $\alpha, \beta > 0$ and functions $y_1, y_2 \in L^1[0, T]$, the following basic properties are satisfied: [36,37]

- **Linearity:**

$$ {}^{\mathrm{C}}\mathrm{D}_t^{\alpha} \big(a y_1(t) + b y_2(t)\big) = a\, {}^{\mathrm{C}}\mathrm{D}_t^{\alpha}\, y_1(t) + b\, {}^{\mathrm{C}}\mathrm{D}_t^{\alpha}\, y_2(t) \tag{9} $$

- **Composition of integrals:**

$$ {}^{\mathrm{R}}\mathrm{I}_t^{\alpha}\ {}^{\mathrm{R}}\mathrm{I}_t^{\beta}\, y(t) = {}^{\mathrm{R}}\mathrm{I}_t^{\alpha+\beta}\, y(t) \tag{10} $$

- **Commutativity:**

$$ {}^{\mathrm{R}}\mathrm{I}_t^{\alpha}\ {}^{\mathrm{R}}\mathrm{I}_t^{\beta}\, y(t) = {}^{\mathrm{R}}\mathrm{I}_t^{\beta}\ {}^{\mathrm{R}}\mathrm{I}_t^{\alpha}\, y(t) \tag{11} $$

These concepts and properties constitute the mathematical basis for applying fractional calculus to optimal control and integro-differential equations. Later sections use these tools to reformulate optimal control problems into nonlinear programming formulations.

3. Fractional dynamics of measles transmission model

In this section, we present a new fractional-order mathematical model for the transmission dynamics of measles that incorporates memory effects through Caputo fractional derivatives and behavioral reactions to vaccination. Fractional calculus has become an effective mathematical tool for modeling real-world biological systems with memory and hereditary characteristics. In the context of infectious disease dynamics, fractional-order derivatives are particularly suitable for representing long-term immunity, delayed behavioral responses to vaccination, and non-local infection effects that depend on past states. These memory-driven features make fractional-order modeling more realistic than classical integer-order approaches. Therefore, we generalized the integer-order measles model of [38] into a fractional-order framework using Caputo derivatives of order $\alpha \in (0, 1]$, defined in Equation (4). This generalization allowed the model to capture both the hereditary nature of measles transmission and the dynamic behavioral responses of individuals, such as vaccine hesitancy or accelerated vaccination during outbreaks. Both these influences were explicitly incorporated into the model, which also enabled the formulation of an optimal control problem aimed at determining cost-effective vaccination and treatment policies. As a result, the new fractional control system was formulated as follows:

$$\begin{cases} \frac{1}{\sigma^{1-\alpha}}\,{}^{\mathrm{C}}\mathrm{D}_t^{\alpha} S(t) = (1-u_1)A - u_2 S - \beta SI - \mu S \\ \frac{1}{\sigma^{1-\alpha}}\,{}^{\mathrm{C}}\mathrm{D}_t^{\alpha} V(t) = u_1 A + u_2 S - u_3 V - \varepsilon\beta\, VI - \mu V \\ \frac{1}{\sigma^{1-\alpha}}\,{}^{\mathrm{C}}\mathrm{D}_t^{\alpha} E(t) = \beta SI + \varepsilon\beta VI - \eta E - u_4 E - \mu E \\ \frac{1}{\sigma^{1-\alpha}}\,{}^{\mathrm{C}}\mathrm{D}_t^{\alpha} I(t) = \eta E - \gamma I - \mu I \\ \frac{1}{\sigma^{1-\alpha}}\,{}^{\mathrm{C}}\mathrm{D}_t^{\alpha} R(t) = u_3 V + u_4 E + \gamma I - \mu R \end{cases} \tag{12}$$

The description of model variables and controls, as well as the interpretation and values of model parameters, is provided subsequently in Tables 1 and 2. The initial values:

$$(S_0, V_0, E_0, I_0, R_0) = (444422, 888844, 80, 60, 9134223) \tag{13}$$

are also referenced from the primary source. [38] Following the introduced approach in, [39] the auxiliary parameter σ was employed to ensure that both sides of the fractional equations in Equation (12) possess the same dimension. This adjustment maintained the dimensional consistency of the fractional system in Equation (12). The diagram of model Equation (12) is given in Figure 1.

3.1. Stability analysis and basic reproduction number

For verifying the stability of the measles transmission model, we considered the following system without control:

$$\begin{aligned} &\frac{1}{\sigma^{1-\alpha}}\,{}^{\mathrm{C}}\mathrm{D}_t^{\alpha} S(t) = A - \beta SI - \mu S \\ &\frac{1}{\sigma^{1-\alpha}}\,{}^{\mathrm{C}}\mathrm{D}_t^{\alpha} V(t) = -\varepsilon\,\beta\, VI - \mu V \\ &\frac{1}{\sigma^{1-\alpha}}\,{}^{\mathrm{C}}\mathrm{D}_t^{\alpha} E(t) = \beta SI + \varepsilon\,\beta\, VI - \eta E - \mu E \\ &\frac{1}{\sigma^{1-\alpha}}\,{}^{\mathrm{C}}\mathrm{D}_t^{\alpha} I(t) = \eta E - \gamma I - \mu I \\ &\frac{1}{\sigma^{1-\alpha}}\,{}^{\mathrm{C}}\mathrm{D}_t^{\alpha} R(t) = \gamma I - \mu R \end{aligned} \tag{14}$$

3.1.1. Existence of disease-free equilibrium

To obtain the disease-free equilibrium (DFE) of the fractional-order system (14), we set the derivatives equal to zero and assumed $E = 0$ and $I = 0$. The algebraic system obtained is:

$$0 = A - \mu S \tag{15}$$

$$0 = -\mu V \tag{16}$$

$$0 = V - \mu R \tag{17}$$

From Equation (15), we get:

$$S = \frac{A}{\mu} \tag{18}$$

The Equation (16) yields:

$$V = 0 \tag{19}$$

and from the Equation (17), we obtain:

$$R = 0 \tag{20}$$

Therefore, the DFE is:

$$(S, V, E, I, R) = \left(\frac{A}{\mu}, 0, 0, 0, 0\right) \tag{21}$$

This equilibrium represents a population entirely susceptible, with no exposed, infectious, or recovered individuals.

3.1.2. Calculation of the basic reproduction number

The basic reproduction number $\mathcal{R}_0$ is a threshold parameter that determines whether an infectious disease can invade and persist in a population. It is the mean number of secondary cases produced by a single infectious individual in a completely susceptible population over the infectious

Table 1. Description of model variables

Variable	Interpretation
$S(t)$	Number of susceptible individuals at risk of infection
$V(t)$	Number of individuals who received the first vaccine dose with partial immunity
$E(t)$	Number of individuals exposed to the virus but not yet infectious
$I(t)$	Number of infected individuals who are infectious and spreading the disease
$R(t)$	Number of recovered individuals or those fully immunized by the second dose or treatment
$u_1(t)$	Proportion of newborns vaccinated with the first dose (early immunization at birth)
$u_2(t)$	Vaccination rate of susceptible adults (delayed or catch-up immunization)
$u_3(t)$	Administration rate of the second vaccine dose ensuring full immunity
$u_4(t)$	Treatment rate of exposed individuals to prevent progression to infectious stage

Table 2. Interpretation and values of model parameters [38]

Parameter	Interpretation	Value	Unit
A	Rate of recruitment (birth of new individuals)	$\frac{10467629}{72.67 \times 12}$	individual/time
β	Effective transmission coefficient	3.0251×10^{-6}	1/(time×individual)
μ	Natural mortality rate	$\frac{1}{72.67 \times 12}$	1/time
ε	Vaccine ineffectiveness factor (first dose)	0.07	–
η	Rate of progression from exposed to infectious class	$\frac{30}{11}$	1/time
γ	Recovery rate of infectious individuals	1.579	1/time

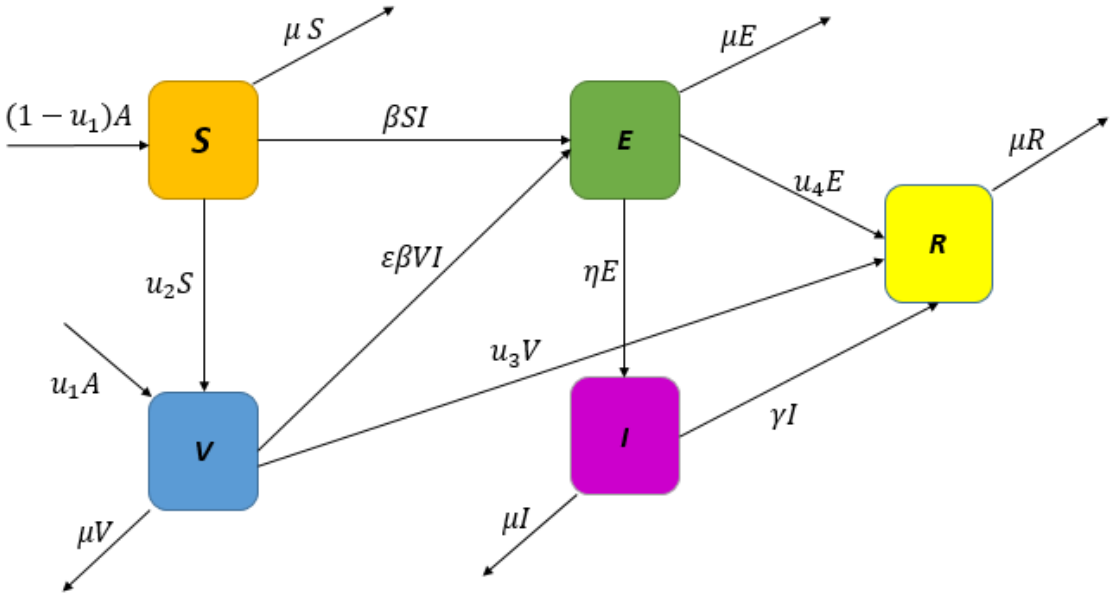

Figure 1. The transmission diagram of measles dynamics

period. To compute $\mathcal{R}_0$ for the fractional-order measles model without controls, we applied the next-generation matrix method, where we took the infected compartments: $E(t)$ and $I(t)$. Let $\mathcal{F}$ represent the rate of new infections, and let $\mathcal{V}$ denote the rate of transfers between compartments:

$$\mathcal{F} = \begin{bmatrix} \beta SI + \varepsilon \beta V I \\ 0 \end{bmatrix} \quad \mathcal{V} = \begin{bmatrix} (\eta + \mu)E \\ -\eta E + (\gamma + \mu)I \end{bmatrix} \tag{22}$$

At the DFE, we have:

$$S = \frac{A}{\mu}, \quad V = 0 \tag{23}$$

The Jacobian matrices of $\mathcal{F}$ and $\mathcal{V}$ with respect to (E, I) at the DFE are:

$$J_{\mathcal{F}} = \begin{bmatrix} 0 & \beta S + \varepsilon \beta V \\ 0 & 0 \end{bmatrix} = \begin{bmatrix} 0 & \frac{\beta A}{\mu} \\ 0 & 0 \end{bmatrix}, \quad J_{\mathcal{V}} = \begin{bmatrix} \eta + \mu & 0 \\ -\eta & \gamma + \mu \end{bmatrix} \tag{24}$$

The next-generation matrix is:

$$K = J_{\mathcal{F}} J_{\mathcal{V}}^{-1} \tag{25}$$

By calculating $J_{\mathcal{V}}^{-1}$ and performing the multiplication, we determine the basic reproduction number as the spectral radius of K by:

$$\mathcal{R}_0 = \frac{\eta(\beta S)}{(\eta+\mu)(\gamma+\mu)} \tag{26}$$

Substituting $S = \frac{A}{\mu}$, we get:

$$\mathcal{R}_0 = \frac{\eta\beta A}{\mu(\eta+\mu)(\gamma+\mu)} \tag{27}$$

It is evident from the above equation how transmission rate, progression rate, recovery rate, and natural death rate affect the spread of the infection within the population.

3.1.3. Stability of the disease-free equilibrium

To examine the local stability of the DFE, we linearized the fractional-order measles system in Equation (14) at the DFE. The Jacobian matrix for the system described in Equation (14) at the DFE is as follows:

$$J_{\text{DFE}} = \begin{bmatrix} -\mu & 0 & 0 & -\beta\frac{A}{\mu} & 0 \\ 0 & 0 & -(\eta+\mu) & \beta\frac{A}{\mu} & 0 \\ 0 & 0 & \eta & -(\gamma+\mu) & 0 \\ 0 & 0 & 0 & \gamma & -\mu \end{bmatrix} \tag{28}$$

To focus on the dynamics of the infected compartments, we defined the infected subsystem (E, I). We considered the corresponding 2×2 Jacobian block J_{EI}, extracted from J_{DFE} in Equation (28). The dynamics of the infected subsystem (E, I) were ruled by the 2×2 block as follows:

$$J_{EI} = \begin{bmatrix} -(\eta+\mu) & \beta\frac{A}{\mu} \\ \eta & -(\gamma+\mu) \end{bmatrix} \tag{29}$$

The characteristic equation of J_{EI} is:

$$\lambda^2 + a_1\lambda + a_0 = 0 \tag{30}$$

where:

$$a_1 = (\eta+\mu)+(\gamma+\mu) > 0, \quad a_0 = (\eta+\mu)(\gamma+\mu) - \eta\frac{\beta A}{\mu} \tag{31}$$

From the definition of the basic reproduction number in (27), we have $a_0 > 0$ if and only if $\mathcal{R}_0 < 1$. Therefore:

- If $\mathcal{R}_0 < 1$, then $a_0 > 0$ and all eigenvalues of J_{EI} have negative real parts, so the DFE is locally asymptotically stable.
- If $\mathcal{R}_0 > 1$, then $a_0 < 0$ and the DFE is unstable.

For the parameter values considered, $\mathcal{R}_0 \approx 0.0064 \ll 1$, all the eigenvalues have negative real parts, and thus the DFE is locally asymptotically stable.

3.1.4. Endemic equilibrium point

To determine the endemic equilibrium point (EEP) of the fractional-order measles model, we considered system (14) and set the derivatives to zero:

$$\begin{aligned} &\frac{1}{\sigma^{1-\alpha}}\,{}^{\text{C}}\text{D}_t^{\alpha}\, S(t) = 0, \qquad \frac{1}{\sigma^{1-\alpha}}\,{}^{\text{C}}\text{D}_t^{\alpha}\, V(t) = 0 \\ &\frac{1}{\sigma^{1-\alpha}}\,{}^{\text{C}}\text{D}_t^{\alpha}\, E(t) = 0, \qquad \frac{1}{\sigma^{1-\alpha}}\,{}^{\text{C}}\text{D}_t^{\alpha}\, I(t) = 0 \\ &\frac{1}{\sigma^{1-\alpha}}\,{}^{\text{C}}\text{D}_t^{\alpha}\, R(t) = 0 \end{aligned} \tag{32}$$

This leads to the algebraic system:

$$0 = A - \beta SI - \mu S \tag{33}$$

$$0 = -\varepsilon\beta VI - \mu V \tag{34}$$

$$0 = \beta SI + \varepsilon\beta VI - (\eta+\mu)E \tag{35}$$

$$0 = \eta E - (\gamma+\mu)I \tag{36}$$

$$0 = \gamma I - \mu R \tag{37}$$

From Equations (33) and (36), we obtained:

$$S = \frac{A}{\beta I + \mu}, \quad E = \frac{\gamma+\mu}{\eta} I \tag{38}$$

From Equation (34), assuming $I > 0$, we determined $V = 0$. Substituting Equation (38) and $V = 0$ into Equation (35) gives:

$$\beta\frac{A}{\beta I+\mu} I - (\eta+\mu)\frac{\gamma+\mu}{\eta} I = 0 \tag{39}$$

Since $I > 0$, dividing both sides by I yields:

$$\frac{\beta A}{\beta I+\mu} = \frac{(\eta+\mu)(\gamma+\mu)}{\eta} \tag{40}$$

After rearranging, we obtain:

$$\beta I + \mu = \frac{\beta A\,\eta}{(\eta+\mu)(\gamma+\mu)} \tag{41}$$

and therefore:

$$I = \frac{\frac{\beta A\,\eta}{(\eta+\mu)(\gamma+\mu)} - \mu}{\beta} \tag{42}$$

Using the definition of the basic reproduction number from Equation (27), we can rewrite Equation (42) as:

$$I = \frac{\mu(\mathcal{R}_0 - 1)}{\beta} \tag{43}$$

Thus, if $\mathcal{R}_0 > 1$, then $I > 0$ and an endemic equilibrium exists, whereas if $\mathcal{R}_0 \le 1$, then $I \le 0$ and no endemic equilibrium exists. Finally, the EEP

is given by:

$$(S, V, E, I, R) = \left(\frac{A}{\beta I + \mu}, 0, \frac{\gamma + \mu}{\eta} I, I, \frac{\gamma}{\mu} I \right) \tag{44}$$

where the variable I is defined in Equation (43), and it is greater than zero if and only if $\mathcal{R}_0 > 1$.

3.2. Sensitivity analysis of the fractional measles transmission model

The basic reproduction number $\mathcal{R}_0$ is one of the determinants of the threshold behavior of infectious diseases. In the case of our fractional-order measles model, the DFE is locally asymptotically stable whenever $\mathcal{R}_0 < 1$, and unstable whenever $\mathcal{R}_0 > 1$. [40,41] Therefore, lowering $\mathcal{R}_0$ below unity is a principal objective for control of epidemic outbreaks. The expression of $\mathcal{R}_0$ obtained in Equation (27) of Section 3.1.2 is composed of effects of some relevant model parameters such as recruitment parameter A, transmission coefficient β, death rate μ, recovery rate γ, and controls u_1, u_2, u_3, and u_4. To evaluate their relative implications, we conducted a local sensitivity analysis. The sensitivity index of $\mathcal{R}_0$ with respect to a parameter p is represented by the following dimensionless formula:

$$\text{Sensitivity index} = \frac{\partial \mathcal{R}_0}{\partial p} \times \frac{p}{\mathcal{R}_0} \tag{45}$$

This equation expresses how the relative change in parameter p affects the relative change in $\mathcal{R}_0$. A positive sensitivity index means that $\mathcal{R}_0$ increases as the parameter increases, whereas a negative sign means an inverse relation. Figure 2 is a bar plot of global sensitivity analysis of the basic reproduction number $\mathcal{R}_0$ with respect to the model parameters. A bar is the normalized sensitivity index of a parameter, illustrating its relative influence clearly. The highest bars represent the recruitment rate A and transmission rate β, both with normalized sensitivity indices of 1.0. This graphic demonstrates a direct proportionality between these two parameters and $\mathcal{R}_0$, confirming that an increase in either will result in an equivalent increase in disease transmission potential. On the other hand, the bar representing u_1, which is newborn vaccination, is negative and is the lowest of all, illustrating the strongest inverse effect on $\mathcal{R}_0$. Moderate negative bars were observed for recovery rate γ and natural death rate μ, which suggests that these parameters are suppressing disease transmission, although to a lesser extent. The remaining control functions u_2 (behavioral intervention), u_3 (second-dose vaccination), and u_4 (exposed individual treatment) had smaller negative contributions. These results point out the value of a synergistic intervention strategy, in which infant immunization takes the lead and is supported by complementary interventions in treatment, awareness, and follow-up vaccination. Table 3 provides a quantitative view through sensitivity indices. Both parameters A and β had sensitivity indices of 1.0000, i.e., an exactly proportional dependence on $\mathcal{R}_0$. This suggests that a 10 % increase in either of the parameters would lead to a 10 % rise in $\mathcal{R}_0$, once again confirming their predominant influence on epidemic dynamics. The control parameter u_1 had the most sensitive inverse effect, with a sensitivity index of -3.5519. This substantial negative value suggests the high effectiveness of newborn vaccination in reducing disease transmission. Other parameters, like recovery rate γ and natural death rate μ, exhibited relatively negative indices, implying enhancement of recovery or decreasing life expectancy by a small measure helps in epidemic control. Behavioral interventions u_2, and partially u_3 and u_4, also had negative indices, affirming their ancillary role in lowering $\mathcal{R}_0$, albeit weaker than that of u_1. Based on the observations in Figure 2 and Table 3, it is clear that focusing on newborn vaccination (u_1) is the most efficient way to lower $\mathcal{R}_0$. This argument is qualitatively asserted by the high-magnitude negative sensitivity index value (-3.5519) and visually corroborated in the bar chart by the prevailing negative bar. Additionally, the statuses of β and A as positively impacting parameters confirm the need to contain transmission channels and population recruitment in the outbreak setting. Although single parameters such as γ, μ, u_2, u_3, and u_4 showed only moderate impact, their combined effect from joint implementation is feasible. Therefore, public health interventions need to focus on high vaccination coverage supplemented by behavioral change and prompt treatment to suppress the disease from successfully spreading and push $\mathcal{R}_0$ below the threshold. Figure 3 is a contour plot of the combined effect of significant control parameters on the basic reproduction number $\mathcal{R}_0$. Level curves on the plot were constant with $\mathcal{R}_0$, and color gradients on the plot indicate the magnitude of variations in matched control measures. This graphical tool makes several significant observations. First, contour lines were densely packed and steeply sloping as u_1 rises, affirming newborn vaccination as the most efficacious intervention for reducing $\mathcal{R}_0$. Second, contour curvature suggested strong interactions among controls—namely, between u_1 and u_2, and between u_1 and u_3. These interactions

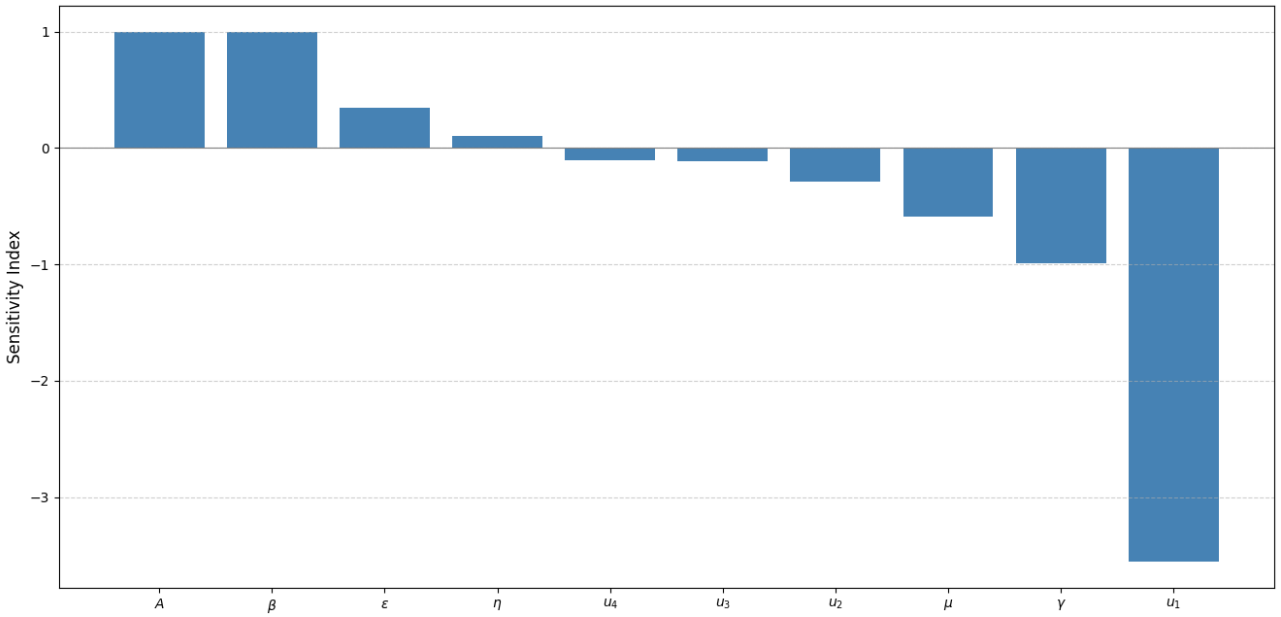

Figure 2. Sensitivity analysis of the fractional-order measles model

indicate that concurrent implementation of vaccination and behavioral interventions has a synergistic effects; hence, $\mathcal{R}_0$ can be decreased at a faster rate than by applying each strategy individually. The second striking observation is the flatness of contours over regions dominated by u_2 and u_4, meaning that such controls, while valuable, must be altered quite significantly to realize a comparable reduction in $\mathcal{R}_0$. Policymakers can therefore use such contour maps to identify cost-effective intervention regions—regions in which modest investment in key controls (such as u_1) results in extensive epidemic suppression. Figure 4 presents a set of surface plots examining the impact on the basic reproduction number $\mathcal{R}_0$ of different combinations of the four control interventions: u_1 (newborn vaccination), u_2 (behavioral intervention), u_3 (second-dose vaccination), and u_4 (treatment of exposed individuals). Here, we can observe how, with rising levels of u_1 and u_2, we experienced a decreasing value of $\mathcal{R}_0$—and that for relatively modest elevations of either variable. A forceful public behavioral response-poster synergism was evident, showing that, according to a surface of negative slope, comparatively slight elevations of these interventions may have extremely substantial epidemiologic effects. In subplot 4bb the combined influence of u_1 and u_3 is shown. Both controls lowered $\mathcal{R}_0$, but the slope of the surface showed decreasing returns with higher levels of u_3. This conclusion implies that second-dose vaccination on its own is less effective unless combined with universal first-dose immunization by u_1. Subplot 4cc investigates the interaction between u_1 and u_4. Here, the decline in $\mathcal{R}_0$ was obvious but less extreme; hence, while treatment of exposed individuals is a complementary intervention, it alone will not be sufficient to control the spread of disease unless newborn vaccination is actually in progress. The last subplot, Figure 4dD, graphs the curve between u_2 and u_3. The surface decreased in $\mathcal{R}_0$ modestly as each parameter increased; hence each has individually favorable effects but not strongly multiplicative ones. Worldwide, the finding confirms that u_1 will be most effective in reducing $\mathcal{R}_0$, especially when reinforced by either a behavioral intervention or a secondary complementary vaccination tactic. The finding is important in planning the best and most cost-effective public health policy. Figure 5 illustrates the influence of key epidemiological parameters on $\mathcal{R}_0$, focusing particularly on combinations of recruitment rate (A), natural death rate (μ), transmission rate (β), and recovery rate (γ). In Figure 5A, when A rises and μ falls, $\mathcal{R}_0$ rises steeply. This suggests that high population inflow with low mortality sustains transmission, the significance of which is emphasized through early-age vaccination in growing populations. Figure 5B also demonstrates that β, the transmission rate, is a primary driver of $\mathcal{R}_0$, especially when mortality μ is low. Any intervention that can lower β—mask wearing, isolation, or mobility restriction—can therefore substantially limit outbreak potential. Figure 5C investigates the relationship between μ and γ. Increasing γ

(recovery) reduces $\mathcal{R}_0$, as expected, and this effect was amplified when increasing μ. This illustration shows the complementary nature of survival time and treatment effectiveness in clearing the disease. These plots reinforce the fact that, although control variables are central to intervention design, biological and demographic parameters significantly impact the underlying disease dynamics and must be accounted for in long-term planning.

4. Optimal control for measles transmission model

Here, we illustrate our proposed control mechanism to minimize the transmission of measles through an optimal intervention process. We intend to decrease the number of patients having measles. We will step-by-step demonstrate how the Hamiltonian equation's requirements solve the problem. We will reformulate this process to maximize the decrease in measles cases.

4.1. Problem formulation for the optimal control problem

The general objective of this work is to determine the optimal intervention measures for measles outbreak control and minimize the related costs. Intervention measures were expressed in the form of four time-dependent controls $u_1(t), u_2(t), u_3(t), u_4(t)$, which are efforts in vaccination and treatment at different levels of the disease. The controls were directed at maximizing vaccination rates and efforts and minimizing the related costs of implementing these efforts. To obtain the optimal control problem, a cost functional was taken into consideration that included intervention cost and the cost of disease burden. The cost functional J is defined as:

$$J = \int_0^T \big[\big(C_1u_1^2(s) + C_2u_2^2(s) + C_3u_3^2(s) + C_4u_4^2(s) + C_5I(s)ds \tag{46}$$

where C_i for $i = 1, 2, 3, 4, 5$ are positive constants that guarantee the balance of each component in the objective function. The first four components in Equation (46) denote the cost of newborn vaccination, first-dose adult vaccination, second-dose vaccination, and medical treatment, respectively. The last component in Equation (46) denotes the cost of the high number of infected individuals in the field, such as media campaign cost, economic cost, etc. The objective was to minimize the cost functional J in Equation (46) by selecting the optimal control strategies $u_1(t), u_2(t), u_3(t), u_4(t)$, while adhering to the fractional-order system of equations presented in Equation (12) and the initial conditions specified in Equation (13).

4.2. Application of pontryagin's maximum principle

To determine the conditions for optimal control of the fractional-order measles model, we applied PMP for systems controlled by Caputo fractional derivatives. The principle allowed us to rewrite the optimal control problem as a boundary value problem in terms of the state equations, the adjoint equations, and characterization of the optimal controls. [11,42–45] We defined the Hamiltonian function H as follows:

$$\begin{aligned} H = {} & \big(C_1u_1^2 + C_2u_2^2 + C_3u_3^2 + C_4u_4^2\big) + C_5I \\ & + \lambda_1\left[(1-u_1)A - u_2S - \beta SI - \mu S\right] \\ & + \lambda_2\left[u_1A + u_2S - u_3V - \varepsilon\beta VI - \mu V\right] \\ & + \lambda_3\left[\beta SI + \varepsilon\beta VI - \eta E - u_4E - \mu E\right] \\ & + \lambda_4\left[\eta E - \gamma I - \mu I\right] \\ & + \lambda_5\left[u_3V + u_4E + \gamma I - \mu R\right] \end{aligned} \tag{47}$$

According to the fractional version of PMP, the adjoint variables satisfy the Caputo fractional differential equations of the form:

$$\begin{aligned} \frac{1}{\sigma^{1-\alpha}}\,{}^{\mathrm{C}}\mathrm{D}_T^{\alpha}\,\lambda_1(t) &= \frac{\partial H}{\partial S} = -\lambda_1(u_2 + \beta I + \mu) \\ &\quad + \lambda_2u_2 + \lambda_3\beta I \\ \frac{1}{\sigma^{1-\alpha}}\,{}^{\mathrm{C}}\mathrm{D}_T^{\alpha}\,\lambda_2(t) &= \frac{\partial H}{\partial V} = -\lambda_2(u_3 + \varepsilon\beta I + \mu) \\ &\quad + \lambda_3\varepsilon\beta I + \lambda_5u_3 \\ \frac{1}{\sigma^{1-\alpha}}\,{}^{\mathrm{C}}\mathrm{D}_T^{\alpha}\,\lambda_3(t) &= \frac{\partial H}{\partial E} = -\lambda_3(\eta + u_4 + \mu) \\ &\quad + \lambda_4\eta + \lambda_5u_4 \\ \frac{1}{\sigma^{1-\alpha}}\,{}^{\mathrm{C}}\mathrm{D}_T^{\alpha}\,\lambda_4(t) &= \frac{\partial H}{\partial I} = -C_5 - \lambda_1\beta S - \lambda_2\varepsilon\beta V \\ &\quad + \lambda_3(\beta S + \varepsilon\beta V) - \lambda_4(\gamma + \mu) + \lambda_5\gamma \\ \frac{1}{\sigma^{1-\alpha}}\,{}^{\mathrm{C}}\mathrm{D}_T^{\alpha}\,\lambda_5(t) &= \frac{\partial H}{\partial R} = \mu\lambda_5 \end{aligned} \tag{48}$$

with the transversality conditions for the co-state equations:

$$\lambda_i(T) = 0, \quad \text{for all } i = 1, \ldots, 5 \tag{49}$$

The method for obtaining the partial derivatives of the Hamiltonian function with respect to

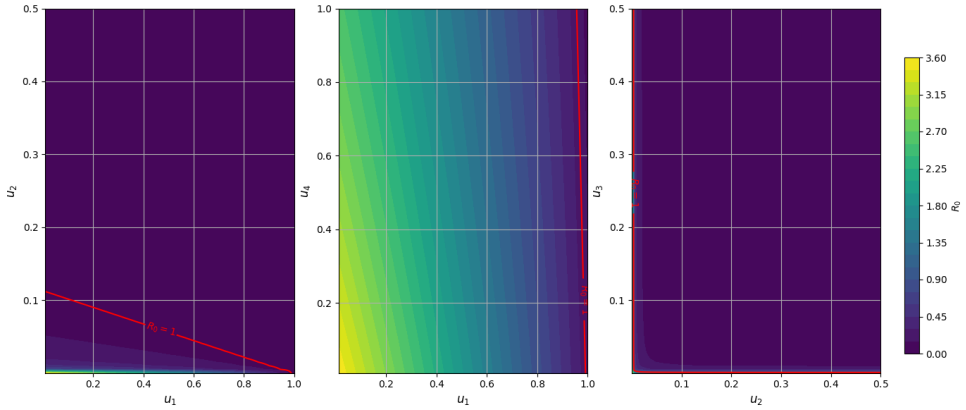

Figure 3. Contour plot of $\mathcal{R}_0$ against key control parameters

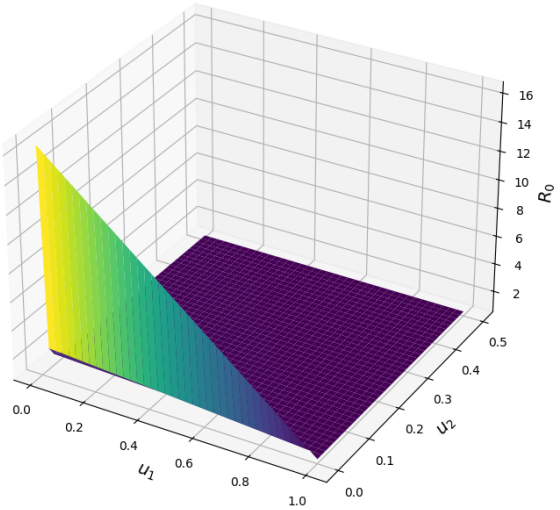

(a) $\mathcal{R}_0$ as a function of u_1 and u_2.

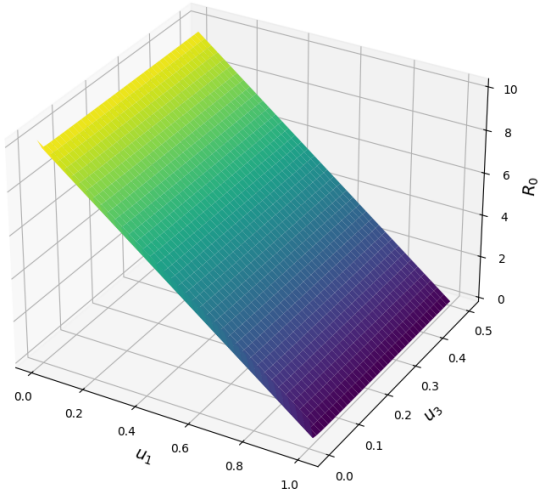

(b) $\mathcal{R}_0$ as a function of u_1 and u_3.

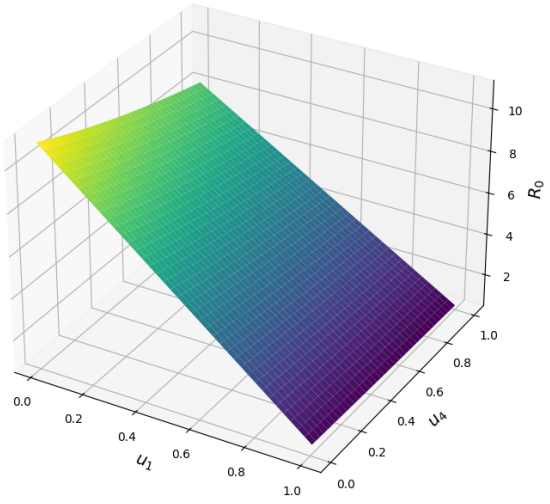

(c) $\mathcal{R}_0$ as a function of u_1 and u_4.

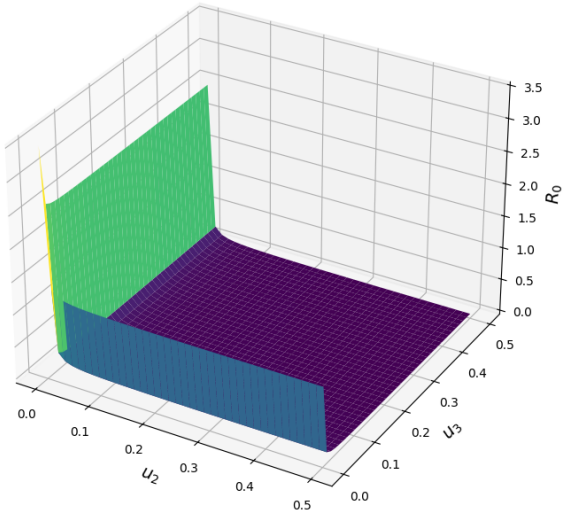

(d) $\mathcal{R}_0$ as a function of u_2 and u_3.

Figure 4. The influence of u_1, u_2, u_3, and u_4 on $\mathcal{R}_0$

Table 3. Sensitivity indices of $\mathcal{R}_0$ with respect to model parameters

Parameter	Index	Parameter	Index
A	1.0000	γ	-0.9894
β	1.0000	μ	-0.5922
ϵ	0.3429	u_1	-3.5519
η	0.1021	u_2	-0.2867
		u_3	-0.1169
		u_4	-0.1025

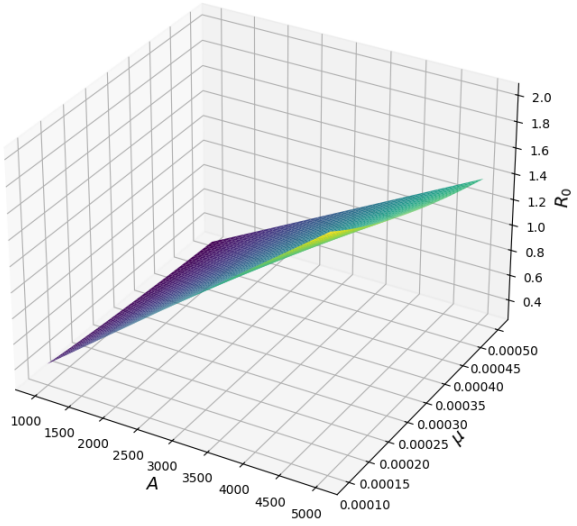

(a) $\mathcal{R}_0$ as a function of A and μ.

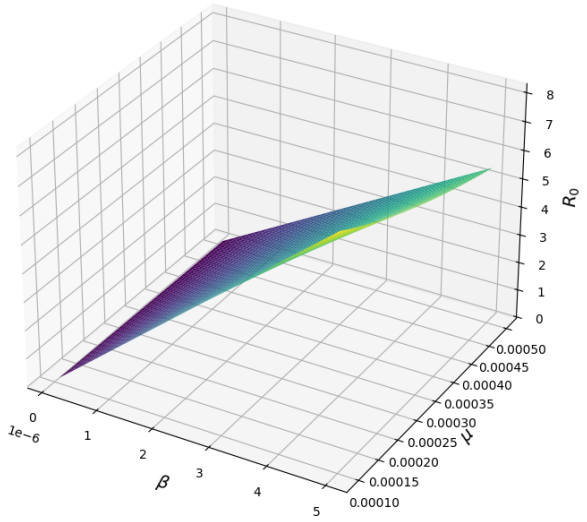

(b) $\mathcal{R}_0$ as a function of β and μ.

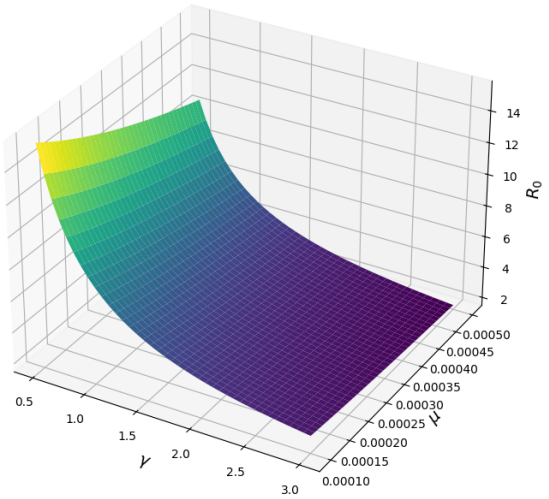

(c) $\mathcal{R}_0$ as a function of μ and γ.

Figure 5. The influence of A, μ, β, and γ on $\mathcal{R}_0$

each costate variable is as follows:

$$\frac{1}{\sigma^{1-\alpha}}\,{}^{\mathrm{C}}\mathrm{D}_t^{\alpha}\,S(t) = \frac{\partial H}{\partial \lambda_1} = (1-u_1)A - u_2 S - \beta S I - \mu S$$
$$\frac{1}{\sigma^{1-\alpha}}\,{}^{\mathrm{C}}\mathrm{D}_t^{\alpha}\,V(t) = \frac{\partial H}{\partial \lambda_2} = u_1 A + u_2 S - u_3 V - \varepsilon\beta V I - \mu V$$
$$\frac{1}{\sigma^{1-\alpha}}\,{}^{\mathrm{C}}\mathrm{D}_t^{\alpha}\,E(t) = \frac{\partial H}{\partial \lambda_3} = \beta S I + \varepsilon\beta V I - \eta E - u_4 E - \mu E$$
$$\frac{1}{\sigma^{1-\alpha}}\,{}^{\mathrm{C}}\mathrm{D}_t^{\alpha}\,I(t) = \frac{\partial H}{\partial \lambda_4} = \eta E - \gamma I - \mu I$$
$$\frac{1}{\sigma^{1-\alpha}}\,{}^{\mathrm{C}}\mathrm{D}_t^{\alpha}\,R(t) = \frac{\partial H}{\partial \lambda_5} = u_3 V + u_4 E + \gamma I - \mu R \tag{50}$$

By differentiating the Hamiltonian function with respect to the control variables, we obtain the following expressions:

$$\begin{aligned}
\frac{\partial H}{\partial u_1} &= 2C_1u_1 - A\lambda_1 + A\lambda_2 \\
\frac{\partial H}{\partial u_2} &= 2C_2u_2 - S\lambda_1 + S\lambda_2 \\
\frac{\partial H}{\partial u_3} &= 2C_3u_3 - V\lambda_2 + V\lambda_5 \\
\frac{\partial H}{\partial u_4} &= 2C_4u_4 - E\lambda_3 + E\lambda_5
\end{aligned} \tag{51}$$

Equating each derivative to zero and applying control bounds, the optimal controls are obtained as:

$$\begin{aligned}
u_1^*(t) &= \min\left\{\max\left[0, \frac{A(\lambda_1-\lambda_2)}{2C_1}\right], 1\right\} \\
u_2^*(t) &= \min\left\{\max\left[0, \frac{S(\lambda_1-\lambda_2)}{2C_2}\right], 1\right\} \\
u_3^*(t) &= \min\left\{\max\left[0, \frac{V(\lambda_2-\lambda_5)}{2C_3}\right], 1\right\} \\
u_4^*(t) &= \min\left\{\max\left[0, \frac{E(\lambda_3-\lambda_5)}{2C_4}\right], 1\right\}
\end{aligned} \tag{52}$$

5. Numerical technique

This section presents a numerical approach for solving the fractional system dynamics given in Equations (50) and (48), which were derived from the application of PMP to the fractional-order optimal control problem in Section 4, by proceeding forward and backward in time. To present this numerical method, we considered a fractional differential equation in the following form:

$$\frac{1}{\sigma^{1-\alpha}}\,{}^{\mathrm{C}}\mathrm{D}_t^{\alpha}\, y(t) = \mathcal{F}(y), \quad y(0) = y_0, \quad t \in [0,T] \tag{53}$$

To solve Equation (53), we used the equivalent integral form based on the Caputo definition:

$$y(t) = \sigma^{1-\alpha}\left(y_0 + \frac{1}{\Gamma(\alpha)}\int_0^t (t-s)^{\alpha-1}\mathcal{F}(y(s))ds\right) \tag{54}$$

We discretized the interval $[0,T]$ into n equal subintervals of length $h = \frac{T}{n}$ and defined the time nodes as $t_j = jh$ for $j = 0,\ldots,n$. Applying the trapezoidal quadrature rule to approximate the integral in (54), we obtained the numerical scheme:

$$\begin{aligned}
y(t_j) = \sigma^{1-\alpha}\Bigg(y_0 + \frac{h}{\Gamma(\alpha)}\sum_{k=0}^{j}\omega_{jk}(t_j-t_k)^{\alpha-1} \\
\mathcal{F}(y(t_k)) + E_j(y)
\end{aligned} \tag{55}$$

where $\omega_{jk} = \frac{1}{2}$ if $k = 0$ or $k = j$, and $\omega_{jk} = 1$ otherwise. Furthermore, the error term $E_j(y)$ satisfies the bound:

$$|E_j(y)| \le \mathcal{B}h^2, \quad \text{where } \mathcal{B} = \frac{T}{12}\max\left|y''\right| \tag{56}$$

Then, the resulting numerical scheme was:

$$y_0 = y(0) \tag{57}$$

$$y_j = \sigma^{1-\alpha}\left(y_0 + \frac{h}{\Gamma(\alpha)}\sum_{k=0}^{j}\omega_{jk}(t_j-t_k)^{\alpha-1}\mathcal{F}(y_k)\right), \quad j = 1,\ldots,n \tag{58}$$

This recursive nonlinear system was solved at each time step using Newton's iterative method to obtain y_j as the approximation of $y(t)$ at t_j. The forward-backward sweep solution method sequentially solved the state and co-state equations derived from the Hamiltonian form of the optimal control problem. Within this procedure, the state Equation (50) is solved forward in time with the initial condition Equation (13), while the adjoint Equation (48) was solved backward in time with the transversality condition Equation (49). The control functions $u_i(t)$ were then adjusted according to optimal conditions after minimizing the Hamiltonian function, as in Equation (52). The convergence and stability of the proposed numerical algorithm for the fractional-order differential system have been examined thoroughly in, [46] thereby ensuring accordingly the reliability of the process in approximating the controlled dynamics of the measles. The subsequent algorithm's steps provide a brief outline of this numerical method.

Algorithm 1. *[1] Set control functions u_1, u_2, u_3, and u_4. Solve the Equation* (50) *with initial condition* (13) *using the same numerical method introduced in this section for the state trajectories in forward time. Solve Equation* (48) *with transversality condition* (49) *using the same numerical method but in backward time for co-state variables. Correct the control function according to Equation* (52) *from the actual state and co-state variables. Verify convergence. If the new state, co-state, and control functions have sufficiently converged to their previous values, terminate; otherwise, go to Step 2.*

6. Simulation and comparative results

For the numerical simulations, we employed the approach presented in Section 5, with implementation carried out in the Python 3.14 software and simulations executed in Visual Studio Code (VS Code v1.105.1).

6.1. Simulation scenarios and cost analysis

We considered six scenarios with varying levels of control to study the impact of control interventions on measles transmission dynamics. All the simulations were carried out using a fractional-order model for various values of the fractional derivative $\alpha \in \{1.0, 0.95, 0.85, 0.75, 0.65\}$. For each scenario and for each value of α, the cost functional J was computed to compare the infection burden with the intervention efforts.

Scenario 1 (No control): All control functions were set to zero: $u_1(t) = u_2(t) = u_3(t) = u_4(t) = 0$. Figure 6 depicts the trajectories of the states of the fractional-order measles model without control interventions for different fractional-order values of α. The dynamics of the susceptible $S(t)$, vaccinated $V(t)$, exposed $E(t)$, infectious $I(t)$, and recovered compartment $R(t)$ are discussed. This discourse provides information regarding the influence of memory effects intrinsic to the fractional-order model on disease progression when there is no mitigation strategy. For the vulnerable fraction $S(t)$, the results show a more precipitous decline in larger values of α, indicating faster loss of the susceptible class as the system approaches classical behavior (i.e., $\alpha \to 1$). Lower values of α slowed down the rate of loss of susceptibility, which is a feature capturing non-local memory effects of fractional dynamics. The exposed class $E(t)$ initially increased, and then decreased. Higher values of α produced a sharper peak and earlier onset of the infectious class, whereas for lower α, the latency period was longer, leading to a delayed peak and spread of the infection. This behavior is in accordance with the fact that fractional derivatives capture long past exposure effects. Within the ineffective compartment $I(t)$, peak height was delayed and amplitude reduced as α decreases. This pattern shows that memory effects possess the ability to lessen outbreak magnitude, but at the cost of increased disease persistence in the population. The standard case ($\alpha = 1$) provides the maximum peak, highlighting the role played by fractional-order to control an epidemic. The vaccinated group $V(t)$ did not change as a result of the lack of control, and the recovered fraction $R(t)$ grew with a rate that is very much dependent on α. With greater α, there was faster accumulation of the recovered, which agreed with increased recovery and spread of the epidemic. Thus, Figure 6 emphasizes the central role played by fractional-order α in determining temporal disease transmission patterns. In the absence of intervention, lower α-systems had slow, long-drawn epidemics with a more gradual peak, while those with α close to 1 followed a faster trajectory. These observations establish the necessity for adjusting control in fractional-order systems since the presence of memory significantly affects the strength and timing of optimal interventions.

Scenario 2 (Full optimal control): All control variables were active and optimally determined using PMP. Figure 7 depicts the state trajectories of the measles transmission model under the full optimal control strategy for various values of the fractional-order α. In this scenario, all control inputs u_1, u_2, u_3, and u_4 were active and derived from the PMP. The state variables $S(t)$, $V(t)$, $E(t)$, $I(t)$, and $R(t)$ were observed over time to understand how the system behaves when subjected to optimal intervention, particularly in relation to the memory effect introduced by the fractional derivative. The susceptible population $S(t)$ exhibited a swift initial decline, subsequently reaching a state of stabilization, with the rate of decrease intensifying as α rises. For higher α, the impact of controls was more immediate, leading to faster reduction in the susceptible pool. The decline was slower at lower α levels, which means that the memory effect slowed down the system's immediate response to changes. For the exposed class $E(t)$, higher α values resulted in a sharp peak followed by a quick drop, reflecting swifted isolation and vaccination responses. As α decreases, the peak shifts to the right and became flatter, implying delayed and more prolonged exposure dynamics due to the fractional memory. The infectious population $I(t)$ was significantly reduced across all values of α, showcasing the effectiveness of the optimal control strategy. Nevertheless, lower α values led to a slightly longer infection period with a broader peak, while $\alpha = 1$ produced the quickest suppression of the epidemic. The vaccinated compartment $V(t)$ increased sharply in all cases, more so for higher α, as the optimal control intensified initial vaccination efforts. This behavior reflects a memoryless system that quickly implements large-scale vaccination, whereas systems with lower α apply control more gradually. The recovered class $R(t)$ also accumulated more rapidly for higher α, indicating a shorter overall epidemic duration. For smaller α, recovery was slower but smoother, again due to the lingering influence of past states. In summary Figure 7 shows that the full optimal control strategy works very well to delay the spread of disease across all fractional-orders. However, its effectiveness and timing were modulated by the order α: higher α accelerates intervention impact, while

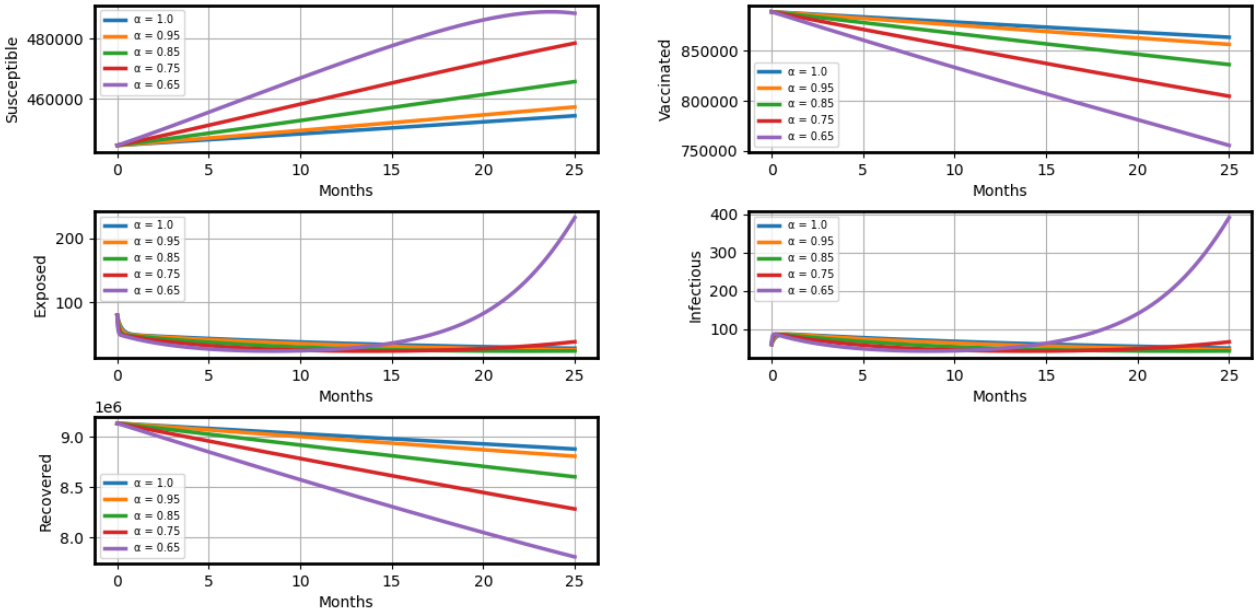

Figure 6. State trajectories for Scenario 1 under different values of α

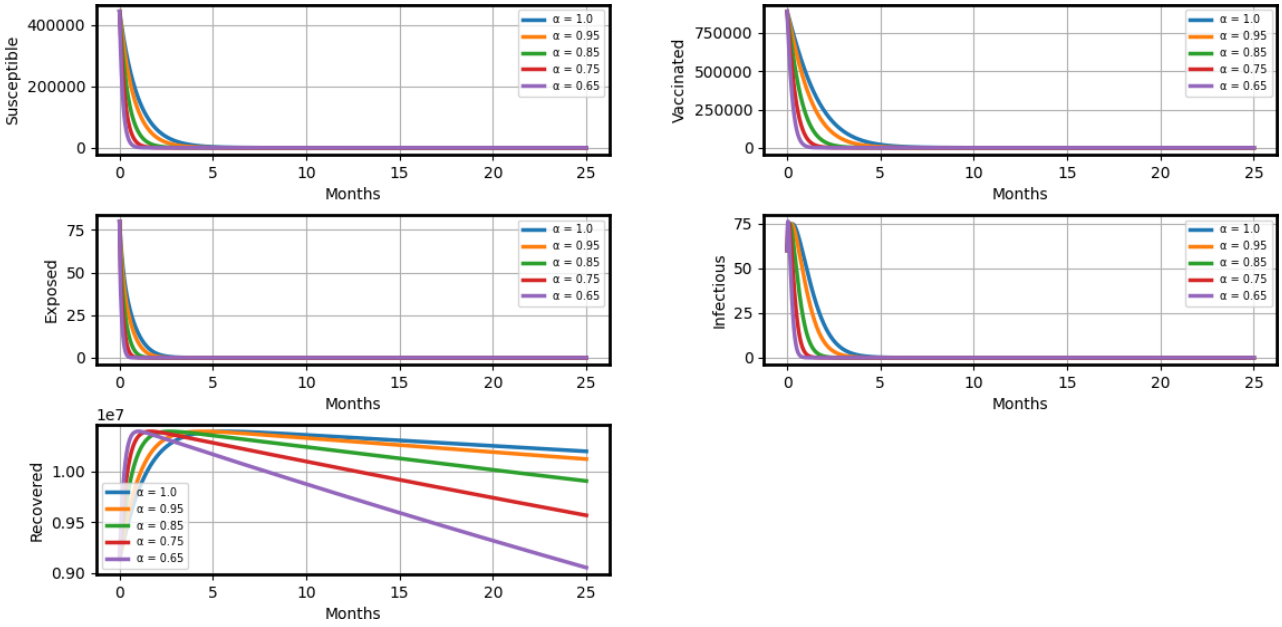

Figure 7. State trajectories for Scenario 2 under different values of α

lower α requires sustained efforts over a longer time horizon. These findings highlight the necessity of tailoring control implementation based on the memory characteristics of the system. Figure 8 is a comparison of model state trajectories under Scenario 1 (no control) and Scenario 2 (optimal control in all) for a given fractional-order $\alpha = 0.95$. The comparison indicates the significant effect of implementing optimal control measures on disease transmission dynamics. In the vulnerable group $S(t)$, Scenario 2 showed a considerably more gradual decline compared to Scenario 1. The outcome revealed the effectiveness of vaccination and campaigns for behavior in checking the susceptible individuals' interaction with infection. Without any control measures, Scenario 1 rapidly depleted the vulnerable population due to unrestricted transmission. For the exposed class $E(t)$, the peak was lower in Scenario 2 and sooner, reflecting that the optimal control policy effectively reduces the rate of new exposures and accelerated transition through the incubation period. In Scenario 1, the higher and later peak of $E(t)$ is a reflection of uncontrolled

spread and a longer latent period. The ineffective population $I(t)$ presented the most dramatic contrast. In Scenario 1, the ineffective population accumulated to a high peak, resulting in a severe outbreak. Under best control (Scenario 2), not only was this peak reduced greatly, but it was also achieved earlier, indicating both control and time delay for the epidemic peak. The vaccinated compartment $V(t)$ was constant in Scenario 1, as one would anticipate when there is no vaccination. In Scenario 2, $V(t)$ increased rapidly over time, demonstrating the significance of proactive immunization in repressing epidemics. Finally, the recovered population $R(t)$ rised more slowly in Scenario 2, as fewer individuals go through the infectious phase due to effective prevention. Scenario 1, however, experienced a sharp increase in $R(t)$ after the peak of infection, illustrating natural recovery in a largely uncontrolled epidemic. This comparative visualization confirms that the enforcement of an entire optimal control plan significantly alleviates rates of infection, delays or reduces peak outbreaks, and limits extended-duration outbreaks of the disease, even in fractional-order models with $\alpha = 0.95$.

Scenario 3 (Newborn vaccination only): Here, newborn first-dose vaccination alone was utilized, i.e., $u_1(t) \neq 0$, $u_2(t) = u_3(t) = u_4(t) = 0$. Figure 9 represents state trajectories of the model under Scenario 3 using only newborn vaccination u_1, and the others u_2, u_3, u_4 were equal to zero. The trajectories were traced for different values of the fractional-order α, displaying how memory affects the system response to partial control. The class of susceptible $S(t)$ decreased with time in all cases but with certain α dependence. Larger values of α resulted in a steeper initial drop of $S(t)$, corresponding to faster vaccination response, and smaller values resulted in a delay induced by stronger memory effects. This phenomenon indicates that fractional systems have longer time frames before control actions may have their fullest impact. The population at risk, denoted as $E(t)$, had a higher α, resulting in a steeper and lower-peaked curve; in contrast, the flat delayed peak produced by a smaller α indicates the influence of memory on controlling incubation dynamics of measles. The ineffective population, denoted as $I(t)$, remained significantly greater than the corresponding population under complete control; however, it eventually dropped below the level of uncontrolled $I(t)$. Its peak depended considerably upon α: increased order lessen it sooner and more strongly. The vaccinated class $V(t)$ increased over time due to newborn vaccination. This compartment increased faster for bigger α, confirming that classical dynamics increase the vaccination effect. Conversely, the increase in $V(t)$ became slower and took longer for fractional-orders smaller than 1. The recovered population $R(t)$ was growing at a slower rate under smaller α, with faster growth for $\alpha = 1$. Overall, the graph verifies that newborn vaccination on its own can be quantitatively beneficial, but its efficacy is regulated by the fractional-orders and is not potent enough to manage the outbreak completely. Figure 10 shows a side-by-side plot of Scenario 3 (only newborn vaccination) and Scenario 1 (no control), both under $\alpha = 0.95$. The side-by-side plot was used to isolate the epidemiological advantage of having only one control component implemented. In the susceptible class $S(t)$, Scenario 3 declined more slowly than Scenario 1, indicating that fewer individuals were entering the exposed class due to effective newborn vaccination. In Scenario 3, the exposed population $E(t)$ reached its highest point earlier and at a lower level. This shows that the timing and severity of transmission were better controlled. The infectious population $I(t)$ also showed marked improvement: the peak was much lower and occured earlier in Scenario 3. This trend reflects the contribution of newborn vaccinations to directly reducing the reservoir of susceptible individuals and indirectly lowering the infection burden. The vaccinated compartment $V(t)$ was flat in Scenario 1 but rose in Scenario 3, indicative of the direct impact of the intervention. Meanwhile, the recovered population $R(t)$ rose less in Scenario 3, in proportion to the fewer infections. In general, the comparison supports that even one-component interventions like newborn vaccination may provide tangible epidemiological dividends. However, their limited focus serves to demonstrate the value of combined, multi-component control methods for more comprehensive epidemic control.

Scenario 4 (Exclusive adult vaccination): Only adult catch-up vaccination was considered: $u_2(t) \neq 0$, $u_1(t) = u_3(t) = u_4(t) = 0$. Figure 11 represents the state trajectories of the model for Scenario 4, where only adult vaccination u_3 was turned on and all other controls u_1, u_2, u_4 were zero. The trajectories were traced for various values of the fractional-order α, illustrating the effect of memory effects on the epidemic dynamics for this partial control strategy. The susceptible population $S(t)$ decreased slowly for all values of α, but more rapidly for higher α. This effect is a sign of the moderate impact of adult vaccination compared to newborn immunization. Due to

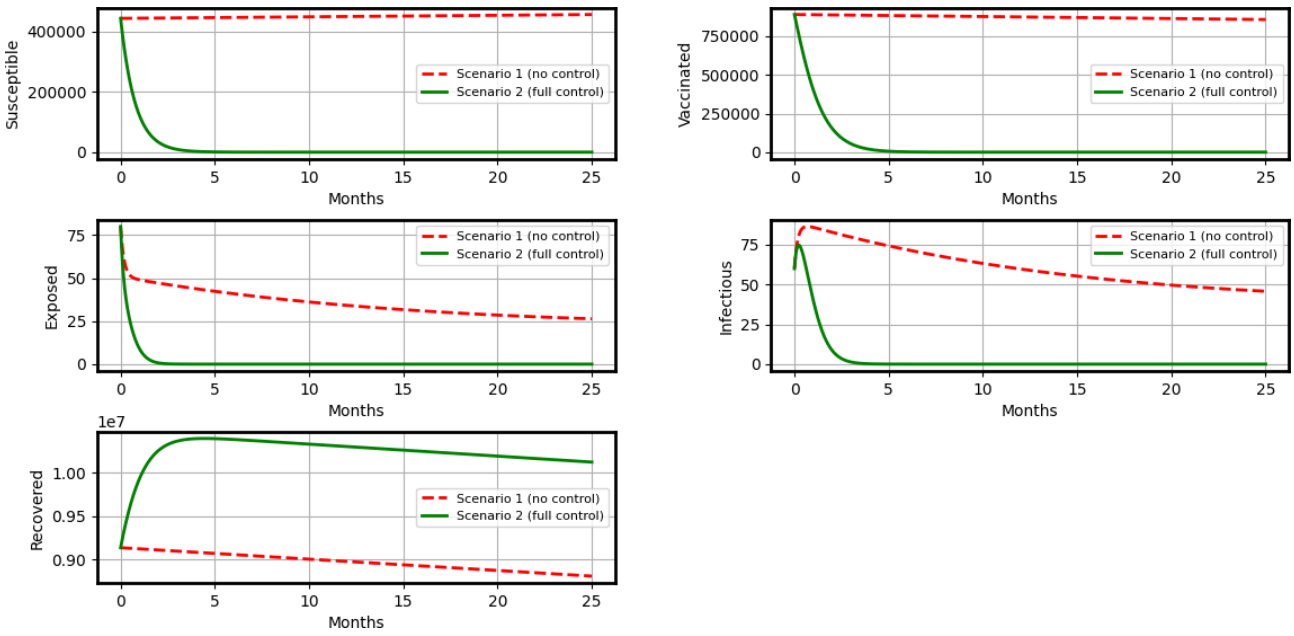

Figure 8. Comparison of the state variables under Scenario 2 versus Scenario 1 for $\alpha = 0.95$

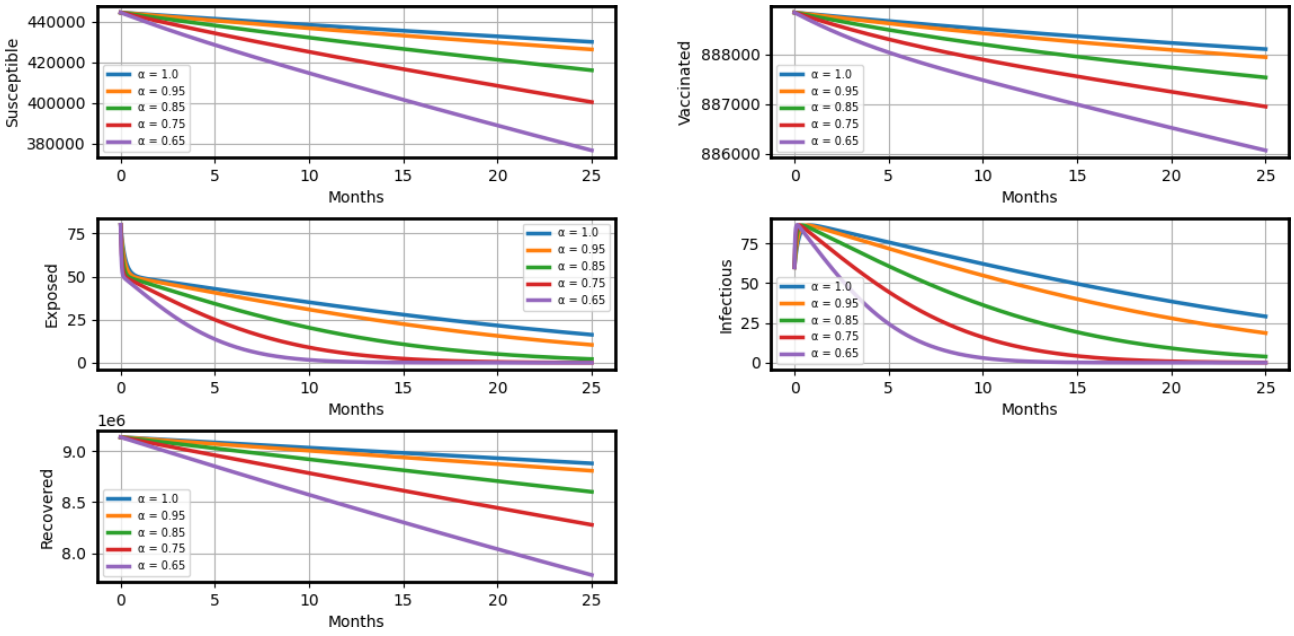

Figure 9. State trajectories for Scenario 3 under different values of α

its delayed nature and low coverage, adult vaccination alone is not sufficient to cause an abrupt reduction in susceptibility. For the exposed population $E(t)$, the curve rose and fell. Larger values of α produced a steeper peak, while smaller values of α postponed the epidemic. This behavior is akin to the memory effect of fractional-order models and the least contribution of u_3 in reducing exposure. In the infectious compartment $I(t)$, adult vaccination led to a reduction in peak height; however, this reduction was not as prominent as that seen with newborn vaccination or full control. Greater values of α still possess superior infection reduction to smaller values, but with less dramatic contrast due to the moderate effectiveness of u_3. The immunized compartment $V(t)$, in this case, representing adult vaccination, increased slowly over time. The rate of growth was higher for larger values of α, and the system response also increased accordingly. The population recovered $R(t)$ rose slowly in all three instances but more quickly for $\alpha = 1$, meaning a quicker transition from infection to recovery in the classical case. Overall, Figure 11 reveals

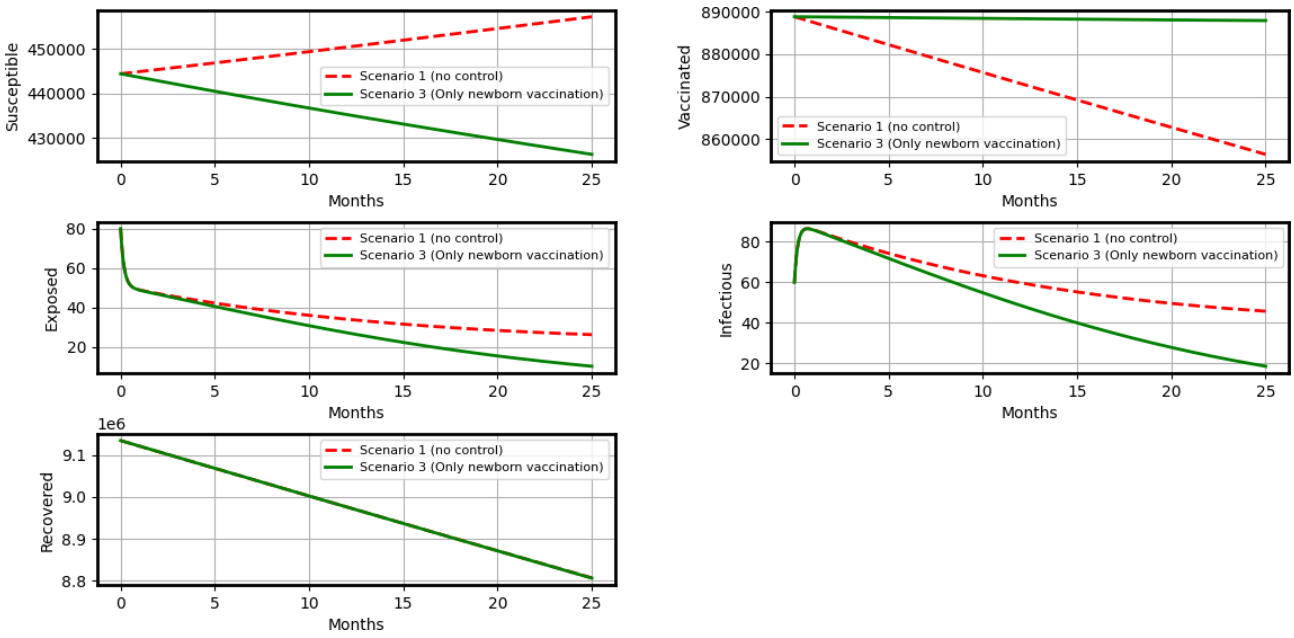

Figure 10. Comparison of the state variables under Scenario 3 versus Scenario 1 for $\alpha = 0.95$

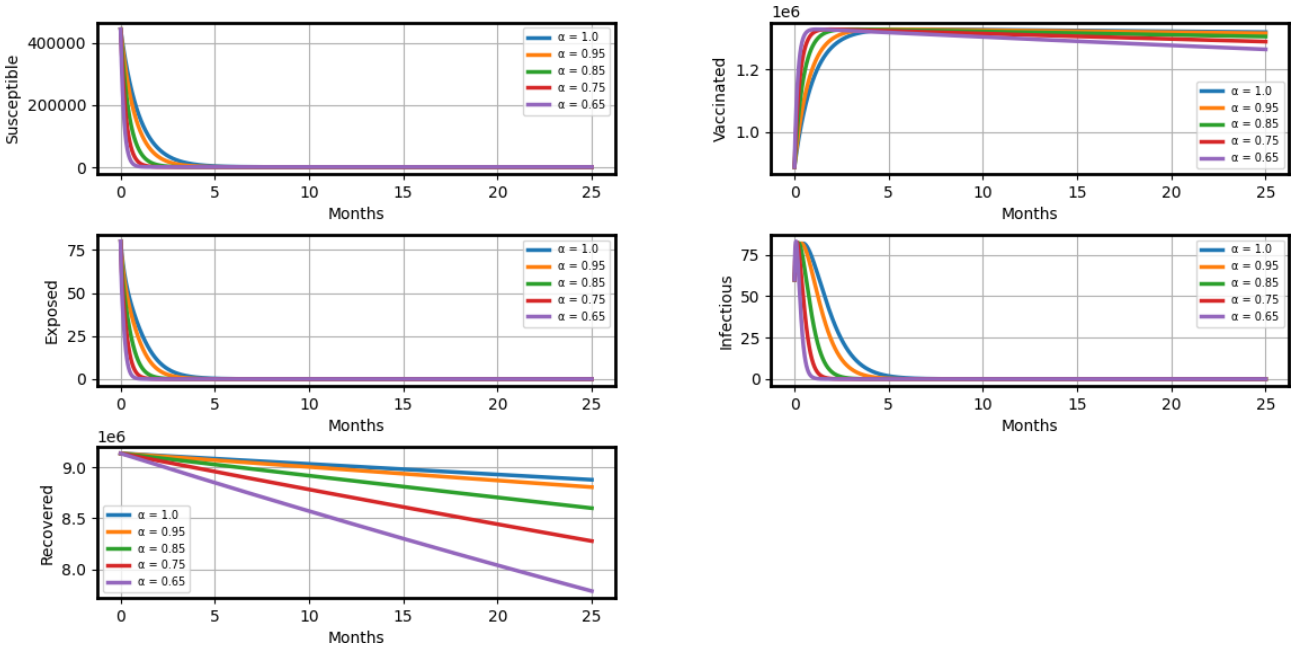

Figure 11. State trajectories for Scenario 4 under different values of α

that while adult vaccination does contribute to disease mitigation, its isolated application has a limited impact. The effectiveness of u_3 was further attenuated under fractional dynamics with lower α, which prolonged disease persistence and reduced control sensitivity. Figure 12 juxtaposes Scenario 4 (u_3 only $\neq 0$) and Scenario 1 (no control) state variables for $\alpha = 0.95$. Juxtaposition aims to quantify the epidemiological benefit of vaccinating adults as an isolated intervention. In the susceptible compartment, denoted as $S(t)$, Scenario 4 showed a slight decrease in the reduction of new exposures compared to Scenario 1, which is consistent with the minor reduction in new exposures resulting from late vaccination. The revealed class $E(t)$ had a marginally earlier and lower peak in Scenario 4, suggesting some decrease in early transmission dynamics. The infectious population $I(t)$ in Scenario 4 had a lower peak height than Scenario 1, but not as spectacularly as in previous scenarios with newborn vaccination or combined interventions. This indicates

that adult-only vaccination moderately represses but does not control outbreaks. In Scenario 4, the population of vaccinated individuals, denoted as $V(t)$, rose continuously, while in Scenario 1, it remained constant, as predicted. The population of recovered individuals $R(t)$ rose at comparable rates in both scenarios, though slightly lower in its terminal value in Scenario 4 due to fewer infections. Finally, Figure 12 confirms that adult vaccination achieves moderate epidemic control gains, especially compared to no intervention. However, adult vaccination alone is insufficient to achieve the target of substantial disease suppression, highlighting the importance of combining it with other public health interventions.

Scenario 5 (Only treatment of exposed individuals): In this scenario, only the control u_4, that is, treatment or quarantine of infected individuals, was activated, and all other controls were set to the zero level. The aim was to determine the separate effect of post-exposure interventions on the global dynamics of measles transmission. Figure 13 illustrates the dynamics of the state variables under Scenario 5 with only the control u_4 (treatment of exposed individuals) applied, while all the other controls u_1, u_2, u_3 were zero. Simulations were carried out for various values of the fractional-order α, and the behavior of the system under partial intervention in fractional-order dynamics was observed. The susceptible population $S(t)$ declined with time in both cases, and the slopes increased more for bigger α. Such a behavior displays a faster process of exposure and infection in less memory-intensive populations. However, since the variable u_4 does not directly affect the susceptible population $S(t)$, its contribution is marginal and indirect. The exposed class $E(t)$ had a moderately dampened peak for larger α, showing that early treatment of the exposed can retard progress to infection. As α is reduced, the peak of $E(t)$ was more delayed and broader, as one would expect for the memory effect prolonging the influence of previous states. The infectious class $I(t)$ was indirectly truncated by efficient control of $E(t)$. However, since no vaccination or behavioral controls were implemented, the suppression is partial. A lower value of α resulted in a later peak that was less pronounced, whereas a higher value of α led to a shorter epidemic duration but a more pronounced peak. The vaccinated population $V(t)$ was constant during this scenario because vaccination was not in effect. The recovered population $R(t)$ increased gradually, with increasingly fast accumulation for increasing α, as would be the case from increasingly fast progress through the infectious class. Overall, Figure 13 shows that treatment of the exposed has a quantifiable but moderate impact when utilized alone. The system's memory also restricted its effectiveness, demonstrating the value of combining it with forward-looking controls such as vaccination. Figure 14 shows the model dynamics under Scenario 5 and Scenario 1 (no control) for a fixed fractional-order $\alpha = 0.95$. We compared the epidemiological effect of implementing only the control u_4. The susceptible population $S(t)$ declined slightly more slowly in Scenario 5, reflecting a slight delay in transmission due to less movement from exposed to infectious. The class that has been exposed to $E(t)$ in Scenario 5 had a smaller and sooner peak, and the result implies that targeting this class can limit their development into active infection. The infectious class $I(t)$ experienced a moderate decline in Scenario 5 with a smaller peak and shorter infectious duration. Lack of vaccination and behavior-oriented interventions limited the overall effect. Constant in both scenarios was the class that has been vaccinated $V(t)$. The recovered population $R(t)$ increased slowly in Scenario 5, since fewer infections occurred due to exposed individuals being treated on time. Despite some gains, the comparison indicates that it does not provide effective protection on its own. In summary, Figure 14 validates that exposing individuals being treated provides modest gains but is not sufficient to impact overall epidemic prevention and needs to be combined with other controls for optimal effect.

Scenario 6 (Full optimal control strategy): In this case, a two-dose vaccine strategy was implemented by activating both infant vaccination u_1 and adult (second-dose) vaccination u_3, and setting the other controls u_2 and u_4 to zero. This setup corresponds to the real-world scenario where vaccination programs try to vaccinate the population in two steps, both infants and adults. Figure 15 displays the evolution of the state variables under Scenario 6 for different values of the fractional-order α. The goal was to evaluate how this dual vaccination strategy influences disease transmission under various memory conditions. The susceptible population $S(t)$ exhibited a pronounced decline as α increased, indicating a swift decrease in susceptibility under classical dynamics. Smaller values of α delayed depletion, illustrating the memory effect of fractional systems in delaying the impact of control policies. The exposed class $E(t)$ had smaller and earlier peaks as α increased. This indicates that two-dose vaccination effectively suppresses exposure, particularly in memory-less systems, while memory delays the

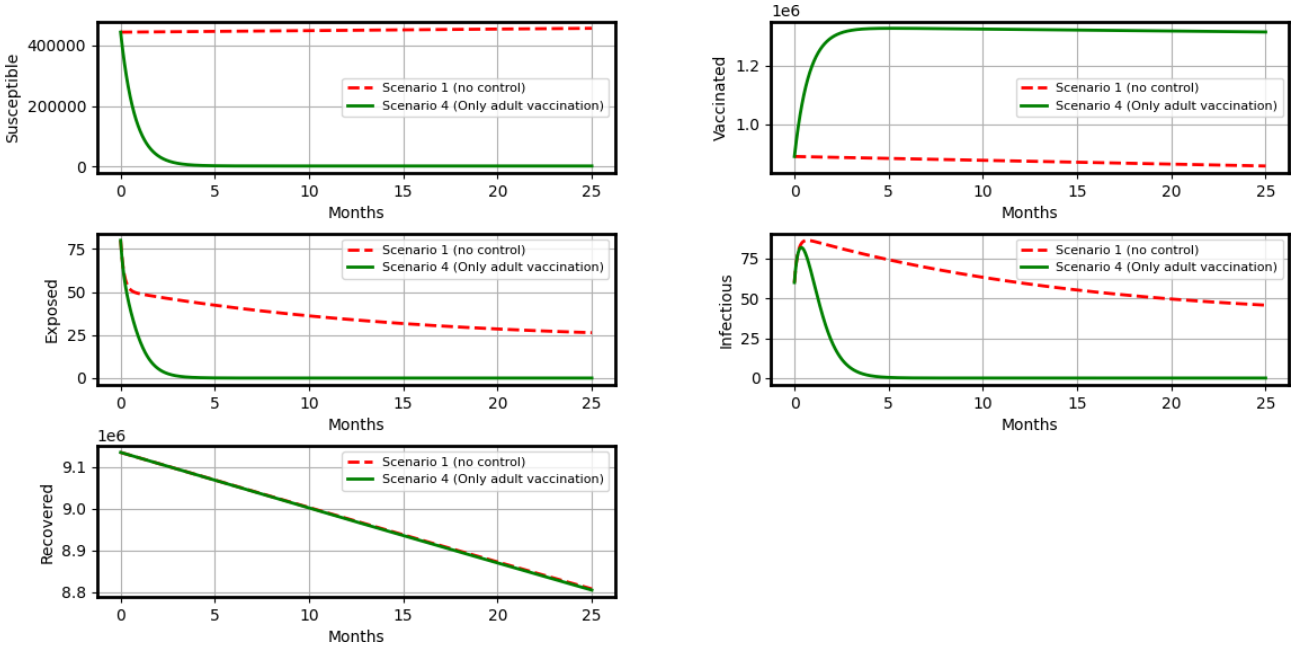

Figure 12. Comparison of the state variables under Scenario 4 versus Scenario 1 for $\alpha = 0.95$

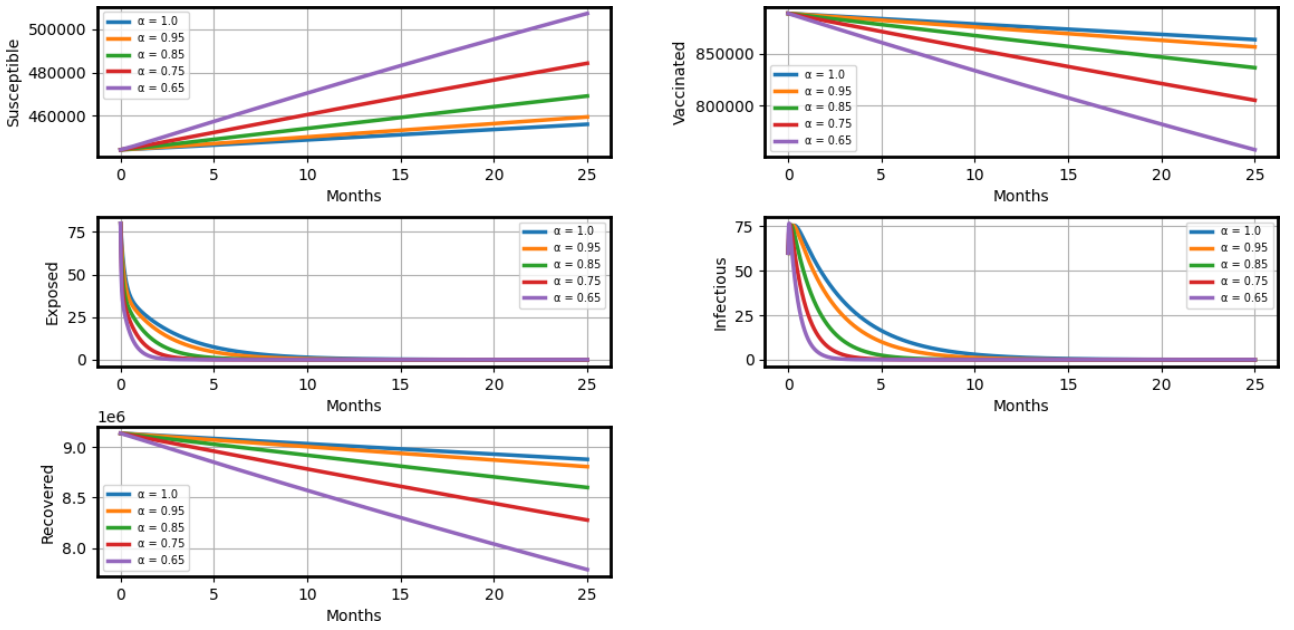

Figure 13. State trajectories for Scenario 5 under different values of α

response. The infectious class $I(t)$ showed a significant reduction for all α cases. The infection peak decreased and narrowed for increasing α, confirming the strong impact of early and repeated vaccination in managing disease spread. The vaccinated class $V(t)$ increased over time and developed faster for larger α, as the system reacted faster to vaccination campaigns. On the other hand, fractional memory introduced a delay for a vaccination to happen. The recovered class $R(t)$ increased more quickly with larger α, consistent with a shorter infectious period and larger recovery flow. Smaller α cases have slower but more gradual growth. Figure 15 thus shows the benefit of combining u_1 and u_3: infant protection initially and follow-up vaccination in older individuals resulted in substantial epidemic reduction over memory values. Figure 16 compares the state variables in Scenario 6 and Scenario 1 (no control), when the fractional-order $\alpha = 0.95$ is fixed. This comparison describes the epidemiological advantage of a two-dose vaccine approach. The susceptible population $S(t)$ declined more gradually in Scenario 6, reflecting the

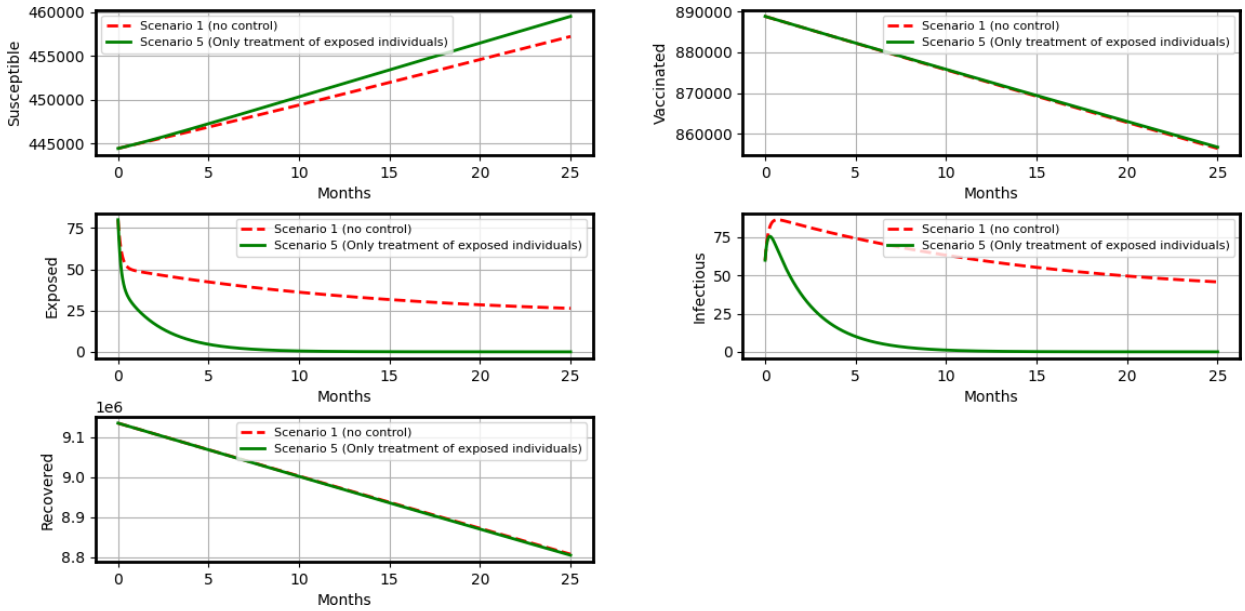

Figure 14. Comparison of the state variables under Scenario 5 versus Scenario 1 for $\alpha = 0.95$

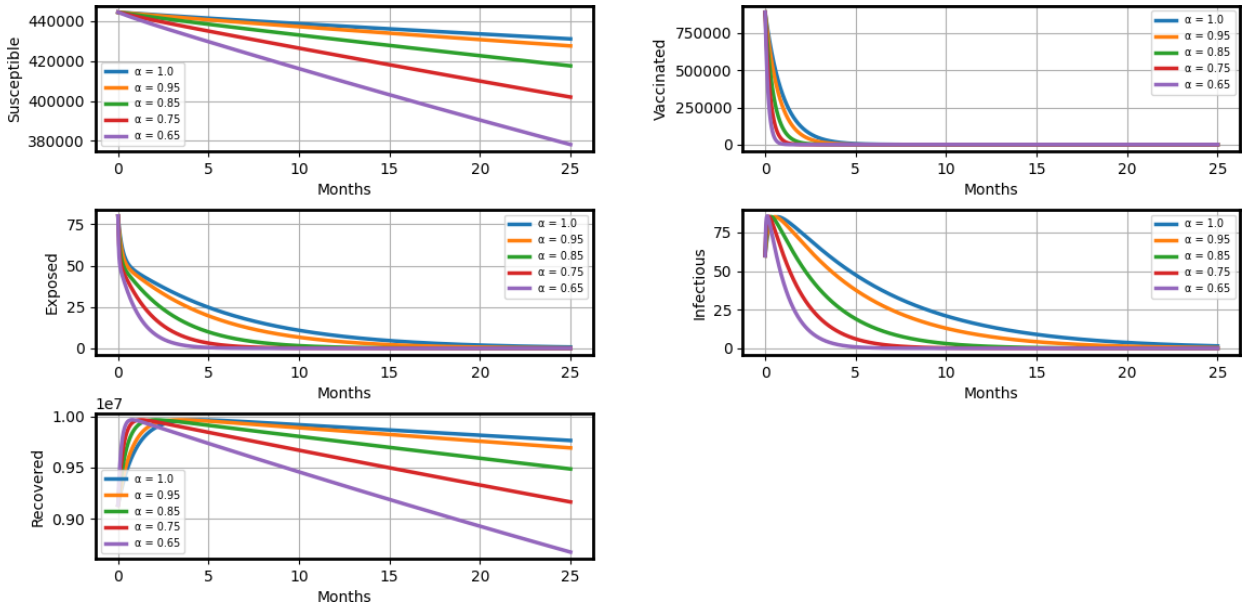

Figure 15. State trajectories for Scenario 6 under different values of α

shielding impact of sustained immunization coverage. Scenario 1 showed susceptibility exhaustion at a faster rate owing to uncontrolled exposure. The exposed class $E(t)$ peaked earlier and lower in Scenario 6, reflecting reduced incidence of exposure from the onset of the epidemic. Similarly, the infected population $I(t)$ in Scenario 6 was significantly lower than in Scenario 1, and its peak was lower and earlier. The vaccinated population $V(t)$ increased linearly in Scenario 6 and remained constant in Scenario 1, as it ought to. The recovered class $R(t)$ had a more gradual buildup in Scenario 6 due to the prevention-based strategy rather than natural recovery. Finally, Figure 16 confirms that the combination of u_1 and u_3 significantly improved epidemic control, even for fractional-order dynamics with $\alpha = 0.95$. The strategy diminishes infection burden, flattens epidemic peaks, and suggests the effectiveness of an exhaustive vaccination campaign.

6.1.1. Comparative summary of scenarios

Table 4 presents a detailed comparison of six different intervention strategies based on three metrics: the maximum number of infectious individuals ($I_{\max}$), the time at which this peak occurs, and the total cost functional (J) for fractional-order $\alpha = 0.95$. Scenario 1 (no control) yielded the worst outcomes, with the highest infection

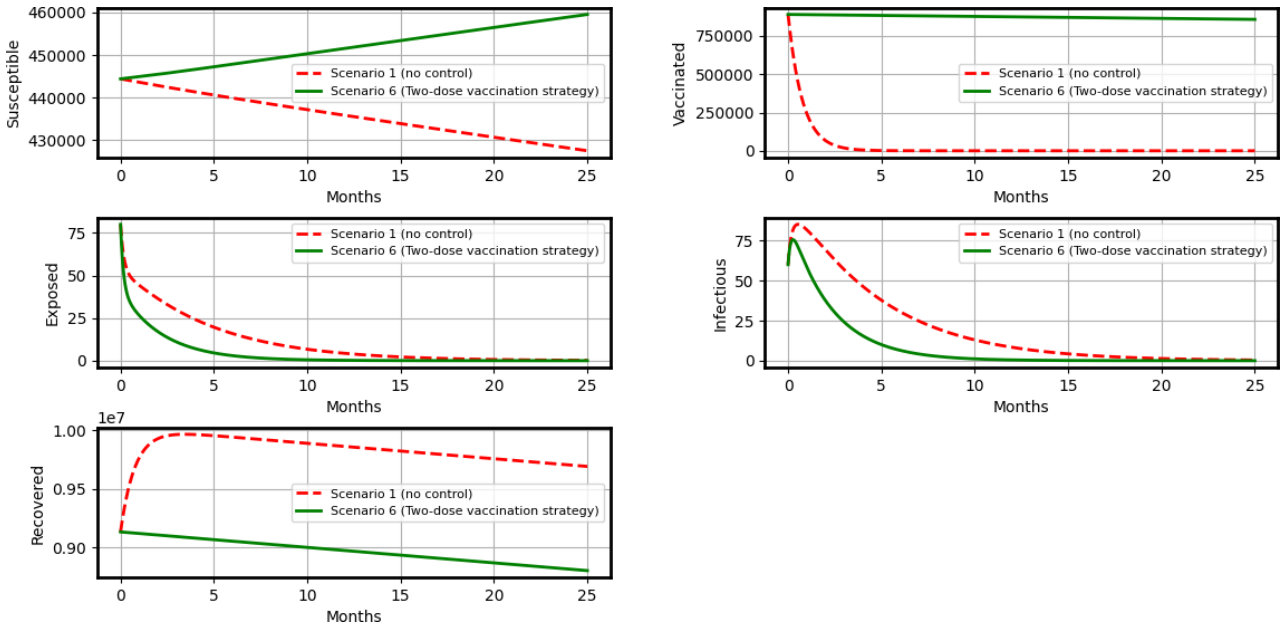

Figure 16. Comparison of the state variables under Scenario 6 versus Scenario 1 for $\alpha = 0.95$

burden and maximum cost. Scenario 2 (full control), on the other hand, had the lowest infection peak ($I_{\max} = 74.77$), the earliest outbreak suppression (peak at 0.23 months), and a very low cost ($J = 2637.74$). This shows how effective it is to use all control measures at the same time. Among the individual strategies (Scenarios 3–5), Scenario 5 (only treatment of exposed individuals) performed better than vaccination-only approaches, reducing both infection burden and cost. Scenario 3, which included only newborn vaccination (u_1), showed minimal improvement over no control. Scenario 6, which combined newborn and adult vaccination (u_1 and u_3), offered a practical middle ground. It achieved a moderate reduction in $I_{\max}$ (85.17) and cost ($J = 14559.73$), suggesting that multi-dose vaccination is a cost-effective alternative when full control is not feasible. In summary, this table highlights the importance of combined interventions—particularly full or two-dose vaccination strategies—as optimal approaches for mitigating the spread and cost of infection under fractional-order dynamics.

6.2. Impact of behavioral response on control strategies

To mimic more natural human behavior dynamics under an epidemic outbreak, the vaccination function $u_1(t)$ and the behavioral control function $u_2(t)$ were assumed to be decreasing sigmoid functions of the infectious population $I(t)$ as:

$$u_1(t) = \frac{u_{1,\max}}{1 + \rho_1 I(t)}, \quad u_2(t) = \frac{u_{2,\max}}{1 + \rho_2 I(t)} \tag{59}$$

Here, parameters ρ_1 and ρ_2 modulate the sensitivity of the control functions to infection intensity and thus can account for behaviorally driven effects such as fear-induced vaccine avoidance or reactive health seeking. Figure 17 depicts how the ineffective population $I(t)$ develops for different values of ρ. With larger values of ρ, implying greater behavioral resistance, the success of the vaccination campaign is compromised, leading to higher peak infections and longer-duration outbreaks. This confirms that strong negative behavioral feedback can highly undermine disease control. Figure 18 plots the shape and dynamics of the behaviorally responsive control function $u_1(t)$. For small values of ρ, the function remains near its elevated level for long times, characterizing stricter and longer public obedience. However, for high values of ρ, $u_1(t)$ rapidly drops in response to higher infections, showing the way misinformation or fear can decrease inoculation rates at the moment when it is most urgently needed. The economic impact of such behavioral effects is summarized in Figure 19, where the total cost functional J is plotted as a function of ρ. An increasing cost was observed as ρ increases, demonstrating how negative behavioral feedback not only exacerbates the health burden but also places a heavy economic burden. The findings emphasize the importance of public health communication interventions to mitigate fear-based resistance and build trust in vaccination campaigns.

Table 4. The spiral movement of piles in soil during the driving process

Scenario	Active controls	$I_{\max}$	Peak Time (month)	J (Cost)
1	None	86.49	0.69	46163.37
2	u_1, u_2, u_3, u_4	74.77	0.23	2637.74
3	u_1	86.46	0.68	37004.58
4	u_3	85.19	0.54	15652.38
5	u_4	75.63	0.26	6041.84
6	u_1, u_3	85.17	0.53	14559.73

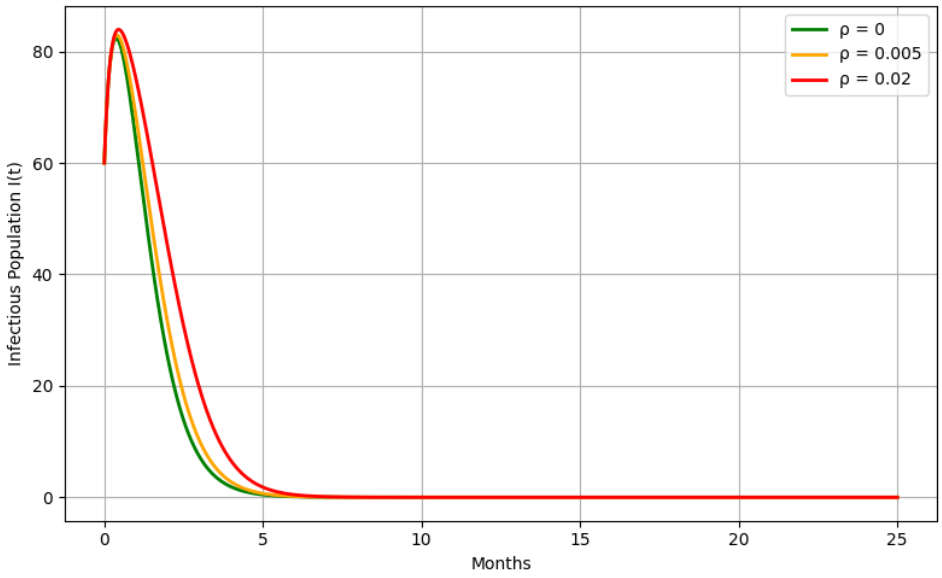

Figure 17. Impact of behavioral response on $I(t)$ for different values of ρ

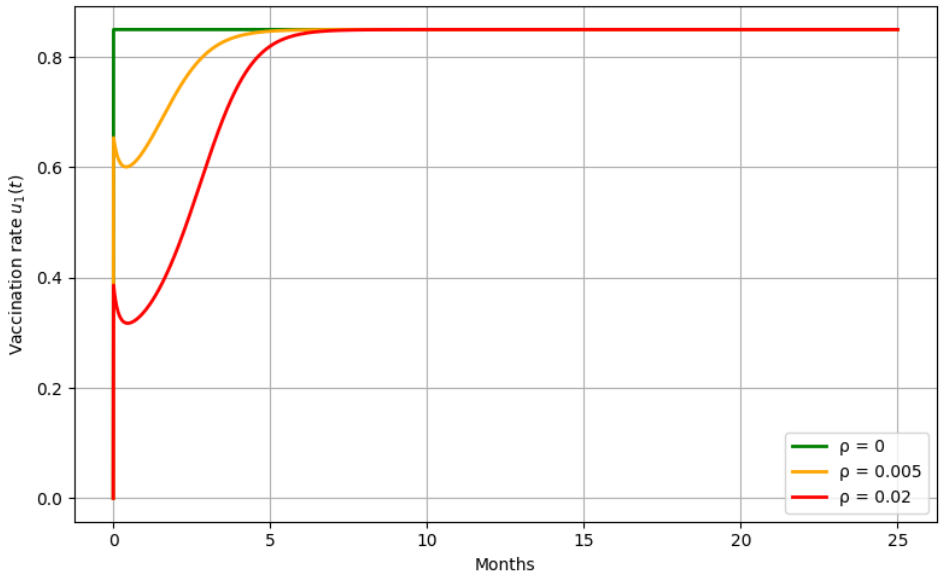

Figure 18. Impact of behaviorally responsive control function $u_1(t)$ under varying ρ

6.3. Cost functional analysis

In this section, we estimated the economic efficiency of different intervention strategies by means of cost-effectiveness analysis. It is a crucial method for guiding public health decisions under stringent resource constraints to achieve maximum benefit for each cost. We estimated the incremental cost-effectiveness ratio (ICER), which

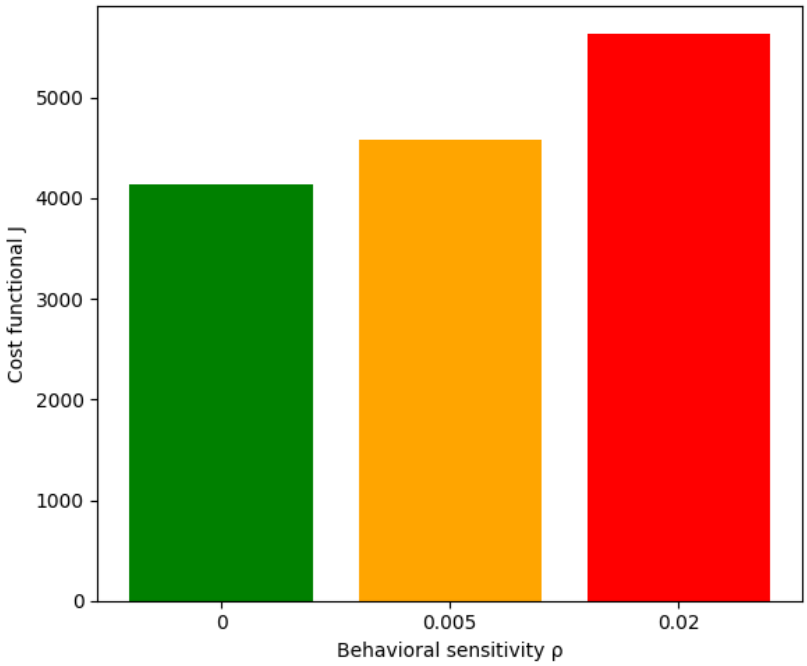

Figure 19. Impact of behavioral response parameter ρ on total cost J

Table 5. ICER for selected scenario pairs with $\alpha = 0.95$

Scenario A	**Scenario B**	$J_A - J_B$	$I_B^{\max} - I_A^{\max}$	**ICER**
2 (Full control)	1 (No control)	-43525.63	11.72	-3712.69
6 (u_1, u_3)	1 (No control)	-31603.64	1.32	-23942.00
6 (u_1, u_3)	2 (Full control)	11921.99	-10.40	-1146.35

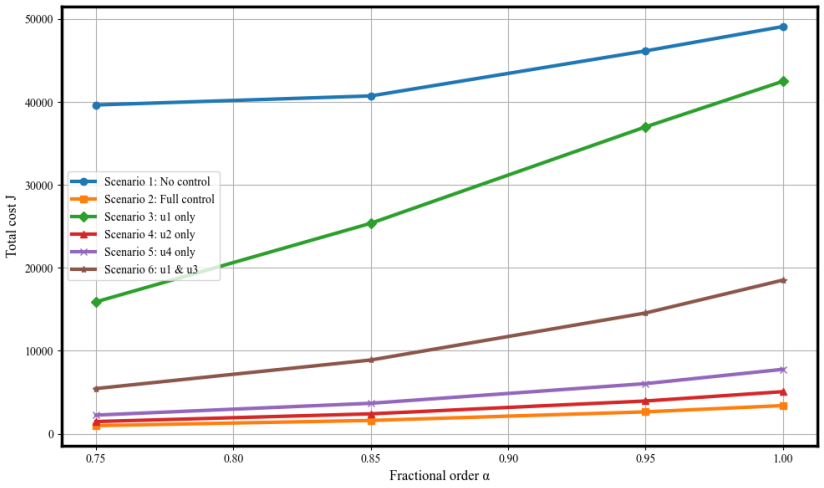

Figure 20. Comparison of total cost J for different control scenarios across various fractional orders α

we set as:

$$\mathrm{ICER}(A, B) = \frac{J_A - J_B}{I_B^{\max} - I_A^{\max}} \tag{60}$$

where J represents the overall cost functional, while $I^{\max}$ denotes the maximum number of infected individuals. The ratio is the incremental cost of avoiding one additional infection when there is a switch from strategy B to A. Table 5 presents ICER values estimated for selected strategy pairs, with Scenario 1 (no control) as the reference and comparison with Scenarios 2 and 6, and a comparison between Scenario 6 and Scenario 2. Absolute and relative cost-effectiveness

information can be derived from these. From Table 5, it is evident that Scenario 2, with complete control, provided the greatest reduction in infections at the lowest cost involved, capturing a highly negative ICER (3,712.69) and showing high cost-effectiveness. Scenario 6, implementing a two-dose vaccination protocol (u_1, u_3), also captured cost-effectiveness but with an even more negative ICER (23,942), although the marginal reduction in infection was lower. When we compared Scenario 6 with Scenario 2, we observed that even though Scenario 6 was less expensive, it also suffered a smaller reduction in infections, yielding a negative ICER (1,146.35) due to the reverse comparison direction. This means that Scenario 6 is more cost-saving but less effective. Overall, the analysis reveals that both full control and targeted multi-dose vaccination strategies offer substantial cost-effectiveness benefits compared to no intervention. Full control is still the best way to avoid infections for the least amount of money. However, Scenario 6 stands out as a practical, mid-cost strategy that still yielded substantial epidemiological benefits—potentially appealing in settings with limited resources. Figure 20 complements this analysis by illustrating the evolution of total cost J across various fractional orders α for all control scenarios. The total cost decreases with higher intensity of control and lower memory effects (larger α). Scenario 2 consistently exhibited the lowest cost across all values of α, followed by Scenario 6, confirming their favorable cost-effectiveness observed in the ICER Table. The shape of the curves further emphasizes how memory effects in fractional systems amplify or reduce the cost gap between strategies.

7. Conclusion and future directions

This study presented a novel fractional-order compartmental model for measles transmission, enriched with multiple intervention strategies including time-dependent behavioral response functions. Our research enhances conventional integer-order models by integrating memory effects characteristic of fractional calculus, thereby more accurately representing the non-local and history-dependent dynamics of infectious disease transmission. Such memory-driven formulations have demonstrated improved accuracy in epidemiological modeling, especially for diseases with complex, long-term dynamics. [35] Through a series of comprehensive numerical simulations, we demonstrated that the fractional-order α has an important effect on the dynamics of disease spread. Lower values of α reflect stronger memory effects, resulting in delayed epidemic peaks and modified control responsiveness. In our comparison of six control scenarios, Scenario 2 (full optimal control) consistently reduced both the number of infected people and the total cost. However, Scenario 6, which implements a two-dose vaccination strategy, also demonstrated high efficiency and cost-effectiveness, making it a compelling alternative when resources are scarce. These insights align well with findings from recent literature. For instance, the studies [22,23] showed that the Atangana–Baleanu–Caputo and Caputo fractional operators better capture real measles dynamics than classical models. Aldila et al. [8] explored the effectiveness of community-driven awareness campaigns, which complements our behavioral response approach. Furthermore, Pang et al. [10] focused on vaccination and cost considerations in optimal control, while our work advances the subject by integrating fractional dynamics and cost-effectiveness metrics such as ICER. Beyond these classical comparisons, our methodology resonates with recent advances in combining collocation methods and metaheuristic optimization algorithms for solving optimal control problems. Jajarmi et al. [47] introduced a coronavirus metamorphosis optimization algorithm with the collocation method to address COVID-19 vaccination control, demonstrating the strength of nature-inspired solvers in epidemic models. Ebrahimzadeh et al. [16] employed a flood-based metaheuristic optimizer in conjunction with collocation methods for a multi-strain COVID-19 model. Recent applications of hybrid fractional frameworks, such as those in, [17,18] and deep learning-enhanced epidemic modeling, [13] show the potential for further innovation. Their success motivates us to augment our model with evolutionary-based optimizers to improve policy design in the face of uncertainty. Overall, our model presents a flexible and realistic tool for evaluating measles mitigation strategies under both epidemiological and economic constraints. It provides significant direction for health policymakers, especially in reconciling disease control with manageable implementation expenses.

For future research, we recommend enriching the model by considering heterogeneous population structures, vaccination hesitancy, [7] time delay in response functions, and stochastic effects. [25] Integrating spatial diffusion processes or network-based interactions may further enhance predictive accuracy. Finally, calibration with real-world incidence data through Bayesian or data-driven estimation techniques would improve the model's practical relevance for disease forecasting and policy design.

Acknowledgments

None.

Funding

None.

Conflict of interest

The authors declare they have no competing interests.

Author contributions

Conceptualization: Amin Jajarmi
Methodology: Asiyeh Ebrahimzadeh
Software: Asiyeh Ebrahimzadeh
Supervision: Amin Jajarmi
Validation: Amin Jajarmi
Writing - original draft: Asiyeh Ebrahimzadeh
Writing - review & editing: Amin Jajarmi

Availability of data

Not applicable.

AI tools statement

All authors confirm that no AI tools were used in the preparation of this manuscript.

References

1. World Health Organization. More than 140,000 die from measles as cases surge worldwide. 2019. Retrieved from: https://www.who.int/news/item/05-12-2019-more-than-140-000-die-from-measles-as-cases-surge-worldwide.
2. World Health Organization. Measles: Fact sheet. 2018. Retrieved from: https://www.who.int/news-room/fact-sheets/detail/measles.
3. Centers for Disease Control and Prevention. *Epidemiology and Prevention of Vaccine-Preventable Diseases*. Hall E., Wodi A. P., Hamborsky J., et al., eds. 14th ed. Washington, D.C. Public Health Foundation, 2021.
4. Patel M, Lee AD, Clemmons NS, et al. National update on measles cases and outbreaks—United States, January 1–October 1, 2019. *Morb Mortal Wkly Rep.* 2019;68(40):893-896.
5. Patel MK, Goodson JL, Alexander Jr JP, et al. Progress toward regional measles elimination—worldwide, 2000–2019. *Morb Mortal Wkly Rep.* 2020;69(45):1700-1705.
6. Bidari S, Yang W. Global resurgence of measles in the vaccination era and influencing factors. *Int J Infect Dis.* 2024;147:107189.
7. MacDonald NE. Vaccine hesitancy: Definition, scope and determinants. *Vaccine* 2015;33(34):4161-4164.
8. Aldila D, Ndii MZ, Samiadji BM. Optimal control on COVID-19 eradication program in Indonesia under the effect of community awareness. *Math Biosci Eng.* 2020;17(6):6355-6389.
9. Edward S, Raymond KE, Gabriel KT, et al. A mathematical model for control and elimination of the transmission dynamics of measles. *Appl Comput Math.* 2015;4(6):396-408.
10. Pang L, Ruan S, Liu S, et al. Transmission dynamics and optimal control of measles epidemics. *Appl Math Comput.* 2015;256:131-147.
11. Ebrahimzadeh A, Jajarmi A, Baleanu D. Enhancing water pollution management through a comprehensive fractional modeling framework and optimal control techniques. *J Nonlinear Math Phys.* 2024;31(1):48.
12. Bansal J, Kumar A, Kumar A, et al. Investigation of monkeypox disease transmission with vaccination effects using fractional order mathematical model under Atangana-Baleanu Caputo derivative. *Model Earth Syst Environ.* 2025;11:40.
13. ur Rahman M, Boulaaras S, Tabassum S, et al. A deep neural network analysis of fractional omicron mathematical model with vaccination and booster dose. *Alexandria Eng J.* 2025;118:435-448.
14. Sweilam NH, Al-Mekhlafi SM, Abdel Kareem WA, et al. A new crossover dynamics mathematical model of monkeypox disease based on fractional differential equations and the Ψ-Caputo derivative: Numerical treatments. *Alexandria Eng J.* 2025;111:181-193.
15. Farman M, Xu C, Abbas P, et al. Stability and chemical modeling of quantifying disparities in atmospheric analysis with sustainable fractal fractional approach. *Commun Nonlinear Sci Numer Simul.* 2025;142:108525.
16. Ebrahimzadeh A, Khanduzi R, Jajarmi A. Collocation method with flood-based metaheuristic optimizer for optimal control on a multi-strain COVID-19 model. *Int J Optim Control Theor Appl.* 2025;15(2):294-310.
17. Eiman, Shah K, Sarwar M, et al. On rotavirus infectious disease model using piecewise modified Atangana–Baleanu–Caputo fractional order derivative. *Netw Heterog Media* 2024;19(1):214-234.
18. Eiman, Shah K, Sarwar M, et al. On mathematical model of infectious disease by using fractals fractional analysis. *Discret Contin Dyn Syst S.* 2024;17(10):3064-3085.
19. Li P, Gao R, Xu C, et al. Dynamics exploration for a fractional-order delayed zooplankton–phytoplankton system. *Chaos Soliton Fract.* 2023;166:112975.
20. Evirgen F, Uçar S, Özdemir N, Jajarmi A. Enhancing maize foliar disease management through fractional optimal control strategies. *Discret Contin Dyn Syst S.* 2025;18(5):1353-1371.
21. Evirgen F, Uçar S, Özdemir N. Mathematical analysis and optimal control of a Caputo fractional diabetes system with parameter identification. *J Comput Appl Math.* 2026;477:117151.
22. Qureshi S, Memon Z. Monotonically decreasing behavior of measles epidemic well captured

by Atangana–Baleanu–Caputo fractional operator under real measles data of Pakistan. *Chaos Soliton Fract.* 2020;131:109478.
23. Qureshi S. Real-life application of Caputo fractional derivative for measles epidemiological autonomous dynamical system. *Chaos Soliton Fract.* 2020;134:109744.
24. Joshi H, Yavuz M. A novel fractional-order model and analysis of cancer-immune system interaction in an avascular environment with an efficient control mechanism. *Comput Appl Math.* 2026;473:116888.
25. Altaf Khan M, DarAssi MH, Ahmad I, et al. The transmission dynamics of an infectious disease model in fractional derivative with vaccination under real data. *Comput Biol Med.* 2024;181:109069.
26. Lenhart S, Workman JT. *Optimal Control Applied to Biological Models.* Chapman and Hall/CRC, 2007.
27. Berhe HW, Makinde OD. Computational modelling and optimal control of measles epidemic in human population. *Biosyst.* 2020;190:104102.
28. Abou-nouh H, El Khomssi M. Towards a viable control strategy for a model describing the dynamics of corruption. *Math Model Numer Simul Appl.* 2025;5(1):1-17.
29. Nkeki C, Mbarie I. On a mathematical model and the efficacy of control measures on the transmission dynamics of chickenpox. *Bull Biomathematics* 2025;3(1):37-61.
30. Agusto F, Leite MC A. Optimal control and cost-effective analysis of the 2017 meningitis outbreak in Nigeria. *Infect Dis Model.* 2019;4:161-187.
31. Aldila D, Handari BD, Widyah A, et al. Strategies of optimal control for HIV spread prevention with health campaign. *Commun Math Biol Neurosci.* 2020;2020:7.
32. Ahmad A, Ali R, Ahmad I, et al. Global stability of fractional order HIV/AIDS epidemic model under Caputo operator and its computational modeling. *Fract Fract.* 2023;7(9):643.
33. Aldila D. Optimal control for dengue eradication program under the media awareness effect. *Int J Nonlinear Sci Numer Simul.* 2023;24(1):95-122.
34. Diethelm K. The Analysis of Fractional Differential Equations: An Application-Oriented Exposition Using Differential Operators of Caputo Type. *Part of the book series: Lecture Notes in Mathematics* (LNM, volume 2004), Springer Nature, 2010.
35. Zhou Y, Wang J, Zhang L. *Basic Theory of Fractional Differential Equations.* World Scientific, 2023.
36. Kilbas AA, Srivastava HM, Trujillo JJ. *Theory and Applications of Fractional Differential Equations.* Elsevier, 2006.
37. Mainardi F. *Fractional Calculus and Waves in Linear Viscoelasticity: An Introduction to Mathematical Models.* World Scientific, 2010.
38. Rahmayani SA, Aldila D, Handari BD. Cost-effectiveness analysis on measles transmission with vaccination and treatment intervention. *AIMS Math.* 2021;6(11):12491-12527.
39. Gómez-Aguilar JF, Rosales-García JJ, Bernal-Alvarado JJ, et al. Fractional mechanical oscillators. *Rev Mex Fis.* 2012;58(4):348-352.
40. Luchko Y, Yamamoto M. General time-fractional diffusion equation: Some uniqueness and existence results for the initial boundary-value problems. *Fract Calc Appl Anal.* 2016;19:676-695.
41. Castillo-Chavez C, Song B. Dynamical models of tuberculosis and their applications. *Math Biosci Eng.* 2004;1(2):361-404.
42. Bourdin L, Trélat E. Pontryagin maximum principle for finite dimensional nonlinear optimal control problems on time scales. *SIAM J Control Optim.* 2013;51(5):3781-3813.
43. Agrawal OP. A general formulation and solution scheme for fractional optimal control problems. *Nonlinear Dyn.* 2004;38:323-337.
44. Heydari MH, Avazzadeh Z. A direct computational method for nonlinear variable-order fractional delay optimal control problems. *Asian J Control* 2021;23(6):2709-2718.
45. Behroozifar M, Habibi N. A numerical approach for solving a class of fractional optimal control problems via operational matrix Bernoulli polynomials. *J Vibr Control* 2018;24(12):2494-2511.
46. Diethelm K, Ford NJ, Freed AD. A predictor-corrector approach for the numerical solution of fractional differential equations. *Nonlinear Dyn.* 2002;29:3-22.
47. Jajarmi A, Ebrahimzadeh A, Khanduzi R. Coronavirus metamorphosis optimization algorithm and collocation method for optimal control problem in COVID-19 vaccination model. *Optim Control Appl Methods* 2025;46(1):292-306.

Asiyeh Ebrahimzadeh *is an Assistant Professor in the School of Basic Sciences, Farhangian University, Tehran, Iran. She received her Ph.D. in Numerical Analysis from the Department of Applied Mathematics at Iran University of Science and Technology, Tehran, Iran; an M.Sc. in Applied Mathematics from the Faculty of Mathematics, K.N. Toosi University of Technology, Tehran, Iran; and a B.Sc. in Mathematics at ValiAsr University of Rafsanjan, Kerman, Iran. Her scientific interests include optimal control, wavelets, integral equations, and orthogonal functions.*

https://orcid.org/0000-0002-4684-7640

Amin Jajarmi *received his B.Sc., M.Sc., and Ph.D. in Electrical Engineering from Ferdowsi University of Mashhad in 2005, 2007, and 2012, respectively. He is currently an Associate Professor in the Department of Electrical Engineering at the University of Bojnord, Iran. His research interests include computational methods for optimal control of nonlinear and fractional-order systems, mathematical modeling with real-world applications, and chaos control and synchronization.*

https://orcid.org/0000-0003-2768-840X

An International Journal of Optimization and Control: Theories & Applications
(https://accscience.com/journal/ijocta)